ZEISS Correlative Workflows for Advanced Packaging Failure Analysis

ZEISS

Seeing beyond

Introduction

Semiconductor packaging technology advancements are enabling improved system performance beyond transistor scaling. However, increasing density and shrinking of interconnects and complex package architectures introduce new challenges for fault isolation, non-destructive imaging, and physical failure analysis workflows. Advances in 3D X-ray microscopy and AI-enabled reconstruction break traditional barriers of throughput, image quality, field of view and resolution. However, these techniques still face challenges in advanced packages where interconnect pitch and size are in micron scale or below and rely on physical failure analysis (PFA).

X-ray microscopy is still relevant in guiding the sample preparation in PFA, such as determining the region of interest and orientation of the cross-section. In addition, the integration of short-pulsed lasers with FIB-SEMs introduces a new paradigm for high throughput, artifact-free sample preparation of semiconductor packages compared to traditional mechanical methods providing access to deeply buried interconnects and subsequent cross-sectional analysis.

ZEISS has developed a novel correlative workflow connecting these two microscopy techniques where 3D XRM guides precise and targeted sample preparation with fs-laser integrated Ga FIB-SEM, reducing sample preparation and analysis from days to hours. This compendium includes recent publications highlighting this workflow and several use cases that enable sample preparation for fault isolation and physical failure analysis.

Originally published in the May/June 2020 issue of Chip Scale Review

Rapid Analysis of Buried 2.5/3D Package Structures

Cheryl Hartfield, Marcus Kaestner, Sasha Mueller, Juan Atkinson-Mora, Ingo Schulmeyer
Carl Zeiss Microscopy

Abstract

Semiconductor packaging plays a key role in the relentless pursuit of better electronic system performance. Diverse package technologies and strategies are advancing next-generation products for smart systems and a connected world, and package engineers have many options for designing the fullest functionality into the smallest footprints for system-in-package (SiP) and system-on-chip (SoC) packages. Recent work shows chiplets can be connected to an active interposer using 150,000 microbumps at 20 µm pitch in a 40 mm x 40 mm 3D package [1]. Additionally, package interconnect dimensions are crossing over into the space dominated by the silicon back end of line (BEOL) dimensions. Hybrid bonding produces some of the smallest package interconnects. Submicron pitches have been demonstrated, as well as the bonding of 300 mm wafers with submicron accuracies [2]. Recent announcements by multiple companies show hybrid bonding is now spreading beyond CMOS imaging sensors (CIS) into dynamic random access memory (DRAM), 2.5D logic, and SoC, with pick and place accuracy requirements ranging from 3-5 µm down to 250 nm, depending on application [3].

The advances noted above present challenges for package fault isolation, process characterization, and failure analysis (FA). Design for test (DfT) and FA strategies need to be paired with new analysis tools to enable fast development of reliable processes and packages. To achieve rapid analysis of buried fine-pitch package and silicon interconnects, a new approach for high-resolution cross-sectional imaging of structures in 3D packages has been developed. It leverages a femtosecond (fs) laser integrated into a focused ion beam scanning electron microscope (FIB-SEM). This article details the capability of this new system for microbump analysis of a 3D stacked-die package.

Package analysis with a laser-integrated FIB-SEM

Some of the most challenging devices for characterization are those used in high-performance computing and artificial intelligence, where packages can be 80 mm in diameter or larger, and the package interconnect pitches are 40 µm and driving smaller [4]. Reconstructed 3D X-ray microscope (XRM) images show the complexity of fine-pitch interconnects in these devices, which becomes evident at successively higher resolutions (Figure 1).

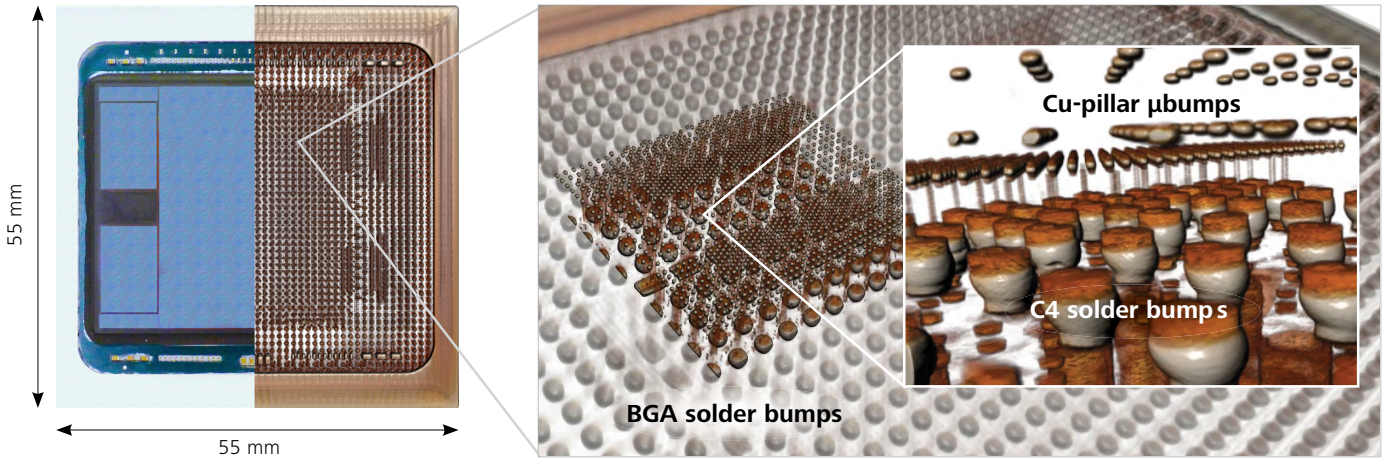

Figure 1 *3D XRM images from three scans of a 55 mm x 55 mm 2.5D package, showing multiple levels of interconnect, the smallest being 25 µm-diameter Cu-pillar microbumps.*

The XRM images are from a delidded, but otherwise fully intact, 55 mm x 55 mm 2.5D package used in an artificial intelligence application. The inset image showing 25 µm-diameter microbumps was acquired using 1.8 µm/voxel. 3D XRM has become standard in FA labs because of its ability to image fully intact packages with high spatial resolution [5], and state-of-the-art 3D XRM has a spatial resolution of 500 nm with voxel sizes of 40 nm [6]. The XRM images are helpful to guide subsequent cross-sectional scanning electron microscope (SEM) analysis.

Si Removal Rate Comparison

Technology	fs-laser (515 nm)*	Xe^+ PFIB**	Ga^+ FIB**
Si Removal Rate	5.4 x 105 µm³/sec	6.7 x 102 µm³/sec	1.0 x 102 µm³/sec
Volume Processed	**Calculated Process Time**		
0.10 mm³	2 seconds	25 minutes	2.8 hours
0.25 mm³	29 seconds	6.5 hours	1.8 days
0.50 mm³	4 minutes	2 days	15 days
0.75 mm³	13 minutes	7 days	49 days
1.0 mm³	30 minutes	17 days	116 days

* Ablation rate used for a high-quality finish
** FIB milling rates based on [15]

Table 1 *Technology timing comparisons for removal of up to one cubic millimeter of silicon.*

Traditional mechanical cross-section techniques are under pressure to deliver artifact-free results at high throughput [7]. Focused ion beam (FIB) processing, while having adequate accuracy and quality for the finest-pitch interconnects, lacks efficiency for removing large volumes of packaging material to analyze buried features.
To address these deficiencies, ZEISS Crossbeam laser was recently developed. It extends the nanoscale imaging and process accuracy of FIB-SEM to packages by enabling site-specific removal of large volumes of packaging material. It includes a fs-laser attached to the external load lock of a gallium ion (Ga^+) FIB-SEM, delivering an improved workflow for site-specific cross-sectional imaging.

Integration of a fs-laser and Ga^+ FIB into a single system ensures a streamlined "cut and look" workflow for fastest time to results, as well as a pristine sample that is not oxidized by exposure to atmosphere, thereby enabling accurate analysis. The fs-laser interaction is essentially athermal [8], producing a laser affected zone (LAZ) smaller than 1 µm under optimized processing conditions. This aids fast Ga^+ FIB polishing times, and rapid results are further enabled by a streamlined single-instrument queue, rather than managing two queues of separate tools.

The laser-integrated FIB-SEM (laserFIB) represents a new class of FIB-SEM, optimized for imaging targeted features at nanoscale resolutions within SiP and 2.5/3D packages. Table 1 shows it is well-suited for removing cubic millimeters of material, unlike the Xe^+ plasma FIB (PFIB). Using parameters for high-quality laser-processed surfaces, it takes four minutes for the fs-laser to remove a half cubic millimeter of silicon, compared to two days for a PFIB or 15 days for a Ga^+ FIB at published milling rates [9].

The time-consuming conventional cross-section steps of epoxy embedding and mechanical polishing are not used in the laserFIB workflow (Figure 2), and if downsizing of larger samples is required, it can be done in areas far away from the desired target location. This reduces the risk of preparation artifacts, even in high-stress packages containing advanced-node silicon die with ultralow K dielectrics.

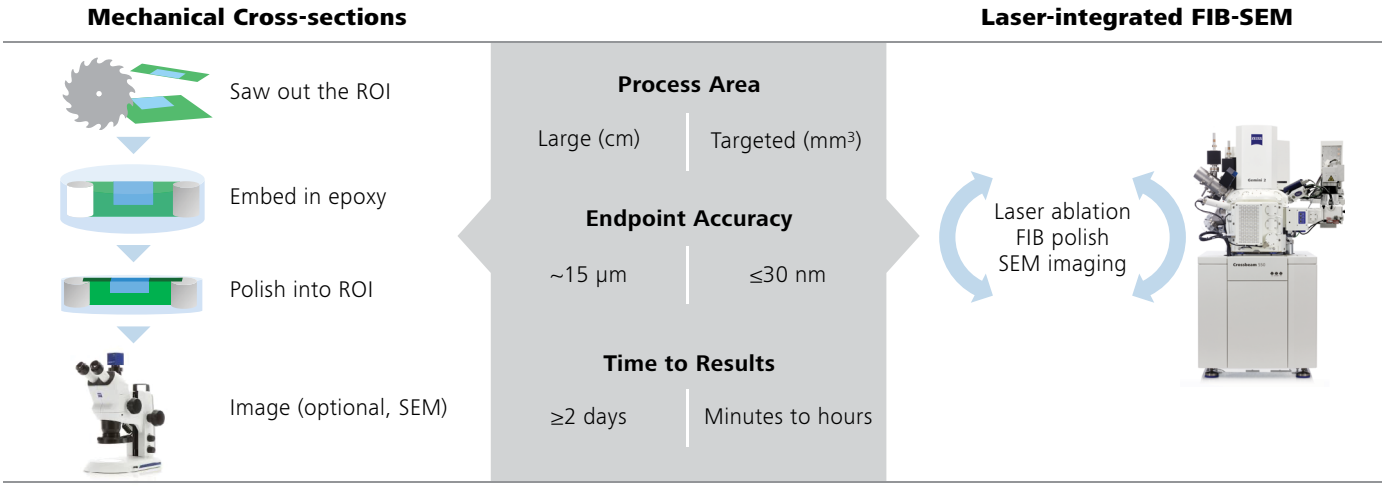

Figure 2 *Cross-section workflow comparisons.*

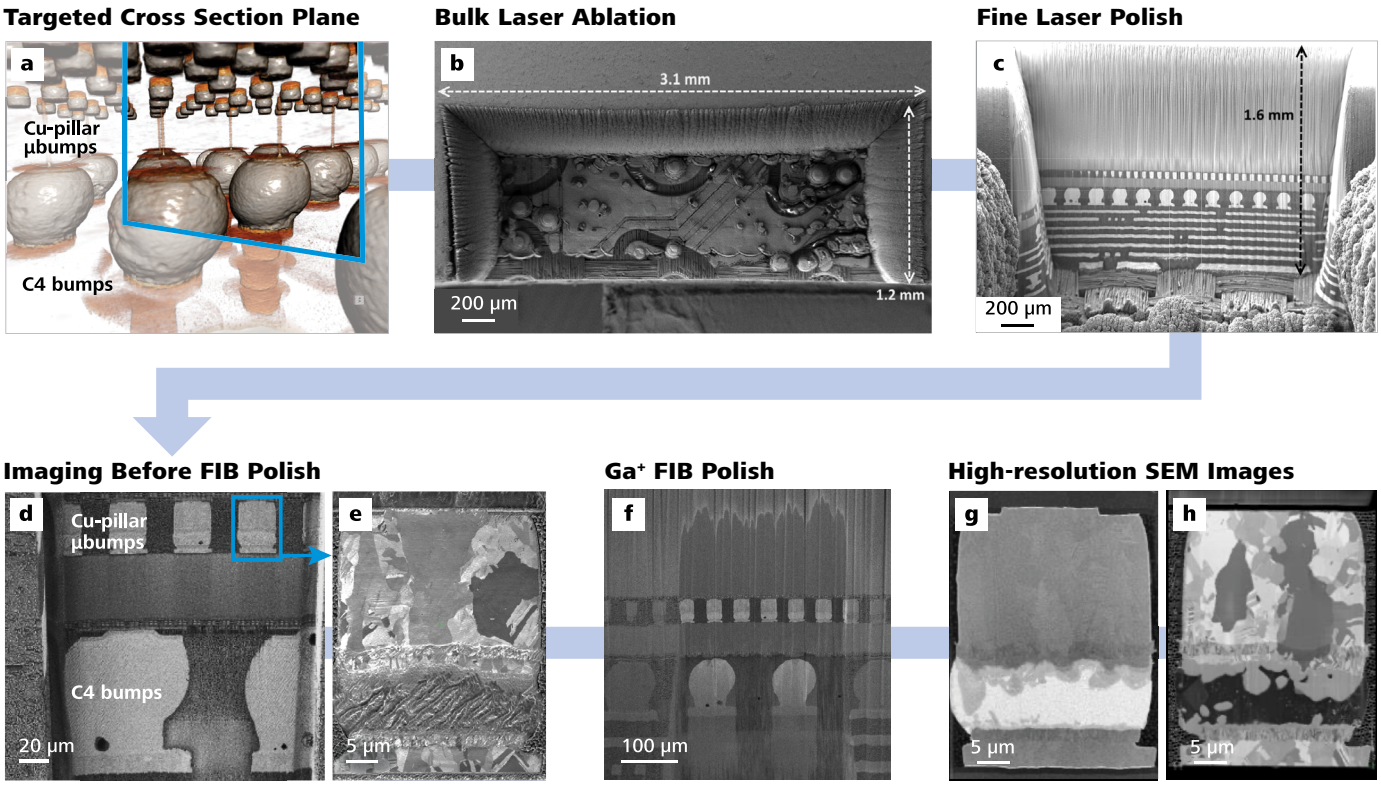

Figure 3 *Steps for correlated 3D XRM and laserFIB analysis of deeply buried microbumps in a 3D package.*

The sloped walls produced by the fs-laser ensure the Ga^+ beam has a short milling path in the z-dimension of this wedge-shaped edge, enabling efficient local Ga^+ FIB polishing and high-resolution imaging across areas of 100 µm to 500 µm wide and equal or greater depths. High imaging quality and low maintenance is ensured by segregating the laser from the FIB-SEM chamber to avoid contaminating the columns and detectors with ablated and recast material. Efficient transfer between chambers enables the repeated cycles of laserFIB processing and imaging that may be required for new recipe set-up or for analyzing multiple sites in a sample.

Cu-pillar microbumps in a 3D package

A laserFIB workflow for imaging 25 µm-diameter Cu-pillar microbumps buried almost one millimeter deep in a 3D stacked-die package is detailed in Figure 3a-h: a) registration of 3D XRM virtual cross-sections to SEM images via the system's software for precise laser pattern placement [10]; b) bulk laser ablation of a large region; c) fine laser polishing; d-e) imaging after the laser polish; f) Ga^+ FIB polishing of a 300 µm-wide local area; g) imaging 25 µm diameter microbumps using high-resolution secondary-electrons; and h) backscattered electrons.

The laser quality allows imaging of some structures right after laser polishing. Ga^+ beam polishing provides the highest-quality surfaces for imaging, removing the shallow LAZ and laser-induced periodic surface structures (LIPSS) to enable imaging intermetallic compounds and other features.

The combined speed and accuracy of the laserFIB has been demonstrated on a 3D package test vehicle for 14 nm node silicon technology. It has 50 µm pitch Cu-pillar microbumps sandwiched beneath a 725 µm thick top die and a 50 µm thick bottom die. Using 1 µm voxel resolution, 3D XRM scans were done at a region of interest. Figure 4 shows a SEM image of the cross-sectioned microbump void superimposed upon the virtual plan-view XRM slice that guided the laser cuts. The void is indicated by a red arrow. The microbump containing the void is circled in the XRM image. The large-area ablation volume was 0.9 x 0.9 x 1.0 mm^3, and the cumulative laserFIB process time to cross-section the void in the microbump was less than one hour, following the workflow described in Figure 3. Both large-area laser ablation and laser fine polishing were completed in 29 minutes. The Ga^+ FIB polishing was done over a 110 µm-wide area that included the affected microbump and progressed until reaching the void. This step took 22 minutes. Therefore, the 5 µm void in the 3D package was accurately cross-sectioned with high quality and no artifacts in less than one hour.

Summary

A laserFIB was used to produce, within one hour, a high-quality cross section of a targeted ~5 µm void within a 25 µm-diameter microbump buried almost 1 mm deep in a 3D package. In comparison, high-quality mechanical cross-sections made through a row of 100 µm-diameter C4 bumps can take more than 2 days [7], and smaller structures like microbumps further reduce throughput and success rates. This work demonstrates that a laser-integrated FIB-SEM enables faster package characterization and FA by enabling rapid access to deeply buried interconnects and interfaces in 2.5/3D packages. The integration strategy enables a streamlined workflow capable of meeting the throughput and success requirements of advanced packages.

XRM Virtual Planar Slice

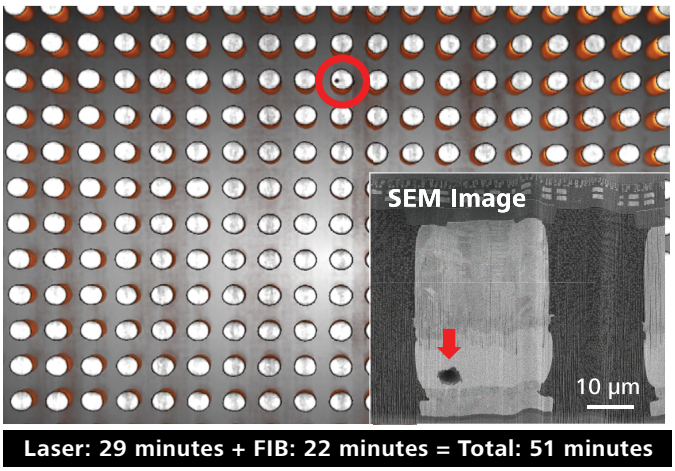

Figure 4 *A 5 µm void (red arrow) found in a single Cu-pillar microbump (red circle) was precisely cross sectioned in less than one hour.*

References

[1] P. Coudrain, et al., "Active interposer technology for chiplet-based advanced 3D system architectures," 2019 IEEE 69th Elec. Comp. and Tech. Conf. (ECTC), 2019.

[2] M. Fujino, K. Takahashi, Y. Araga, K. Kikuchi, "300 mm wafer-level hybrid bonding for Cu/interlayer dielectric bonding in vacuum," Japanese Jour. of Applied Physics, vol. 59, no. SB, 2020, doi: 10.7567/1347-4065/ab4b2b.

[3] L. Mirkarimi, "The Proliferation of Hybrid Bonding for 3D Integrated Circuits," presented at the 3D & Systems Summit, Dresden, 2020.

[4] J. Ryckaert, E. Beyne, "A 3D technology toolbox in support of system-technology co-optimization", imec Magazine, 2019.

[5] C. Hartfield, C. Schmidt, A. Gu, S. T. Kelly, "From PCB to BEOL: 3D X-ray microscopy for advanced semiconductor packaging," Inter. Physics of Failure Analysis, Marina Bay Sands Conv. Center, Singapore, 2018.

[6] ZEISS Xradia 610 and 620 Versa Product Information, version 1.1. (2019).

[7] P. S. Pichumani, F. Khatkhatay, "Mechanical milling and polishing of cross sections using a micro CNC machine for failure analysis," Electronic DeviceFailure Analysis (EDFA), 14-19 (2020).

[8] K. Sugioka, Y. Cheng, "Ultrafast lasers—reliable tools for advanced materials processing," Light: Science & Applications, vol. 3, no. 4, pp. e149-e149, 2014, doi: 10.1038/lsa.2014.30.

[9] S. J. Randolph, J. Filevich, A. Botman, R. Gannon, C. Rue, M. Straw, "*In situ* femtosecond pulse laser ablation for large volume 3D analysis in scanning electron microscope systems," Jour. of Vacuum Science & Tech. B, vol. 36, no. 6, 2018, doi: 10.1116/1.5047806.

[10] J. Favata, V. Ray, S. Shahbazmohamadi, "Correlative 3D X-ray, laser ablation, and SEM/EDS mapping establishing access point for FIB tomography of defects in multi-layer ceramic capacitors," Microscopy and Microanalysis, vol. 25, no. S2, pp. 344-345, 2019, doi: 10.1017/s1431927619002459.

Originally Published with ECS 2022: Proceedings from the 242nd Electrochemical Society Meeting

Emerging Technologies for Advanced 3D Package Characterization to Enable the More-than-Moore Era

C. Hartfield, W. Harris, A. Gu, and M. Terada
Carl Zeiss Microscopy LLC, 5300 Central Parkway, Dublin, California, 94568, USA

V. Viswanathan and L. Jiao
Research Microscopy Solutions Carl Zeiss Pte Ltd, 80 Bendemeer Road, #10-01, 339949 Singapore

T. Rodgers
Carl Zeiss Microscopy GmbH, Carl-Zeiss-Straße 22, 73447, Oberkochen, Germany

Abstract

The line between packaging and silicon interconnect technology is blurring due to a reduction in package interconnect dimensions, which drives an increase in image resolution requirements. It is becoming more difficult to localize and image defects and structures throughout the packaging life cycle, from materials selection, through package and silicon design co-optimization, development, production, and field failure diagnostics. Characterization and failure analysis (FA) solutions must provide fast results for rapid development of packages meeting the required electrical, mechanical and reliability specifications with high yield and quality. Heterogeneous integration and complex packages containing multiple die drive new approaches to rapidly characterize structures, defects and processes. This paper presents new artificial intelligence (AI) developments in 3D X-ray microscopy (XRM) for non-destructive submicron-resolution imaging of packages. It also introduces the latest developments in focused ion beam (FIB) microscopes adapted with an integrated fs-laser for precise and fast analysis of deeply buried features in advanced packages.

Introduction

In the past, the main function of a semiconductor package was to protect the integrated circuit while providing a way to move the signals into a printed circuit board. In recent years, the package has evolved into a critical component providing dense off-chip integration for highest system performance and the extension of Moore's Law. There is a requirement in advanced packaging for 3D interconnects at fine pitch and high density (Figure 1). This is driven by the heterogeneous integration required for high performance computing and mobile devices across a vast array of industries, including IOT, 5G, AI, RF/analog, and automotive. Package interconnect scaling has crossed over into interconnect dimensions formerly only found within die-level BEOL circuitry. Microbumps in 3D packages are 8,000 times smaller than solder balls, and 124 times smaller than C4 bumps, while package I/O pitch is approaching 1 µm [1].

Package designs become 3D by adding more layers, decreasing layer thicknesses, and stacking die. Advanced 3D packages are also incorporating the latest silicon technologies. At the die level, there are efforts to develop backside power delivery networks to address the resistance issues that arise from scaling [2]. As both sides of the die are metallized, even more challenges are introduced to isolate faults and access a buried region of interest, characterize structures and regions of interest in 3D, collect sufficient data, and perform FA without creating artifacts or missing or destroying the region of interest. New advancements in 3D XRM for non-destructive imaging and FIB microscopes for package-level sample preparation bring significant capabilities to package characterization and physical failure analysis.

Advanced Microscopy Innovations For 3D Package Analysis

New packages are developed through a series of learning cycles to enable material selection, design and co-optimization with silicon-level processes, development of multiprobe test technologies, and final products meeting performance and reliability specifications. The push and pull dance between package characterization capability and emerging package technology requirements has existed since the package was first invented. X-ray inspection is one of the oldest package analysis techniques, and C-mode scanning acoustic microscopy (C-SAM) became widespread after the 1980's due to industry adoption of JEDEC standards addressing "popcorn cracking" defects in moisture-sensitive packages [4]. C-SAM has been challenged by the increasing numbers of thin layers and die stacking in 3D packages, and its application has become limited, driving research into GHz techniques [4, 5]. This leads to stronger reliance on X-ray imaging for non-destructive package analysis.

As X-ray inspection has moved from 2D to 3D, the analysis time has increased. To enable 3D data at a suitable intersection of resolution and throughput, different types of 3D X-ray techniques have evolved. These include microcomputed tomography (microCT), X-ray laminography (sometimes called 2.5D X-ray), and X-ray microscopy (XRM), which are described later in this paper.

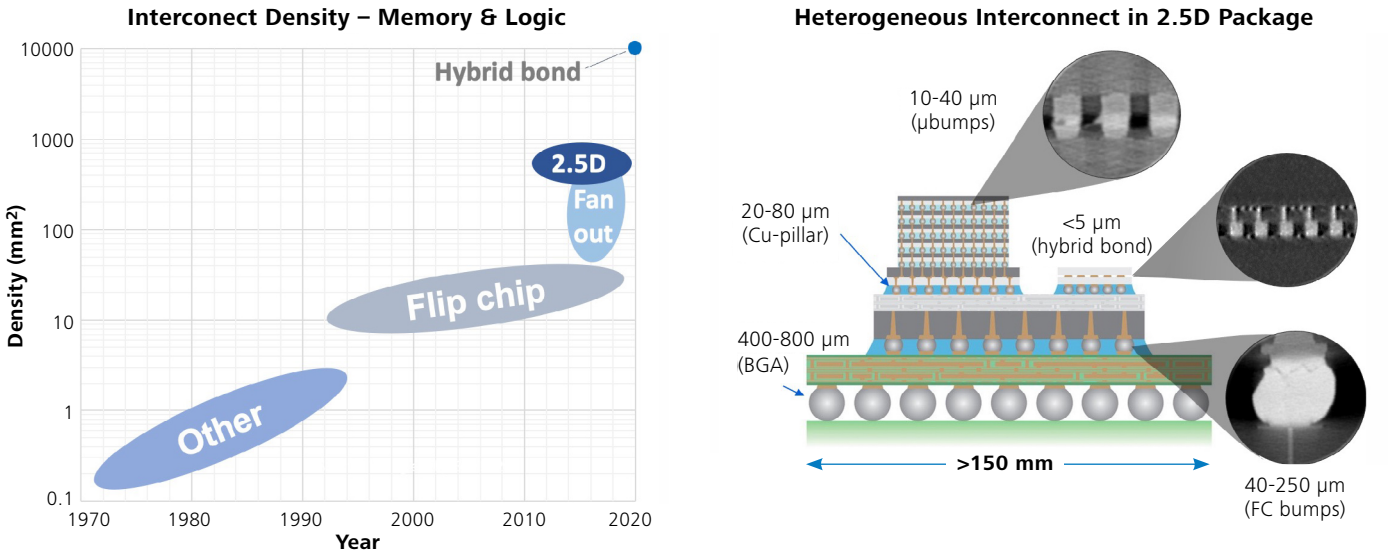

Figure 1 *The density of package interconnect has accelerated in recent years [3] and now approaches 1 µm pitch, with highest densities occurring in hybrid bond technology (left). Interconnects of different types and pitches co-exist in 2.5/3D packages, some of which can be ≥150 mm diameter or larger (right). The zoomed views are virtual slices of 3D XRM data (not shown to scale).*

When it comes to destructive physical failure analysis (PFA), the requirement for artifact-free cross sections of packages and their fast-shrinking structures drives the use of ion beam technologies. This includes broad ion beams (BIB), which are typically Ar, and plasma focused ion beams (PFIB), typically Xe. Advances in packaging technology are pushing BIB and PFIB beyond their limits, due to the combined need for precise end-pointing and rapid site-specific removal of millimeter volumes of material. Broad ion beams can be applied to large areas but lack the end-pointing specificity required by today's advanced fine-pitch high density interconnect. While the traditional Ga FIB and Xe PFIB typically used for semiconductor analysis allow end-pointing on the nanometer scale, both are unable to deliver the milling rates needed for rapid site-specific cross-sectional analysis of structures deeply buried within heterogeneous 2.5/3D and SiP packages.

Advances in 3D X-ray Imaging

Introduction to 3D X-ray Imaging Techniques

X-ray imaging is a transmission microscopy technique, and the composition and size of the sample affect parameters such as scan time, achievable resolution, contrast, and the interplay amongst these variables. To acquire a 3D X-ray image, a sample is placed between an X-ray source and a detector. The sample is automatically rotated to different angular positions, and projection images are collected at the different angles before being reconstructed into a 3D image. For microCT, a flat-panel detector is used, and principles of geometric magnification mandate placing the sample as close as it can get to the source to achieve the highest magnification (Figure 2a). If the magnification becomes limited by a sample size that requires a longer working distance, then resolution will also be limited as a function of the sample size.

Often in microCT, the sample must be cut to a small size to enable the highest-resolution imaging. Semiconductor package dimensions can range from <1 mm on a side up to >150 mm, and advanced packages use wafer-level packaging. To enable 3D X-ray imaging at submicron resolution on large samples, 3D XRM was introduced (Figure 2b). It has a geometric magnification component, and it also incorporates optical magnification by implementing scintillator-coupled objective lenses as detectors. Optical magnification enables high magnification and therefore high resolution when the sample is far away from the source, regardless of the sample size (Figure 2c). In the example shown in Figure 2c, a comparison of microCT and XRM results is shown for a package approximately 40 mm in diameter. While microCT delivers poor resolution for this large sample size, XRM with optical magnification can still resolve fine details within the structure.

X-ray laminography is an X-ray imaging method that emerged to scan packages and printed circuit boards fast at relatively low resolutions. It has a configuration that allows scanning a high aspect ratio sample by passing the beam only through the short axis and avoiding the long axis. This is shown in Figure 3a, where the X-ray beam always takes a short path through the package. This scanning strategy unfortunately causes streak artifacts in the non-planar views when the images are reconstructed (Figure 3b and Figure 3c). For this reason, it is sometimes referred to as 2.5D X-ray microscopy, as it does not provide true 3D images. Laminography can be fast, yet only collection of full angular coverage scans as achieved by microCT or XRM can deliver isotropic 3D spatial resolution by having complete information for the tomographic image reconstruction [6].

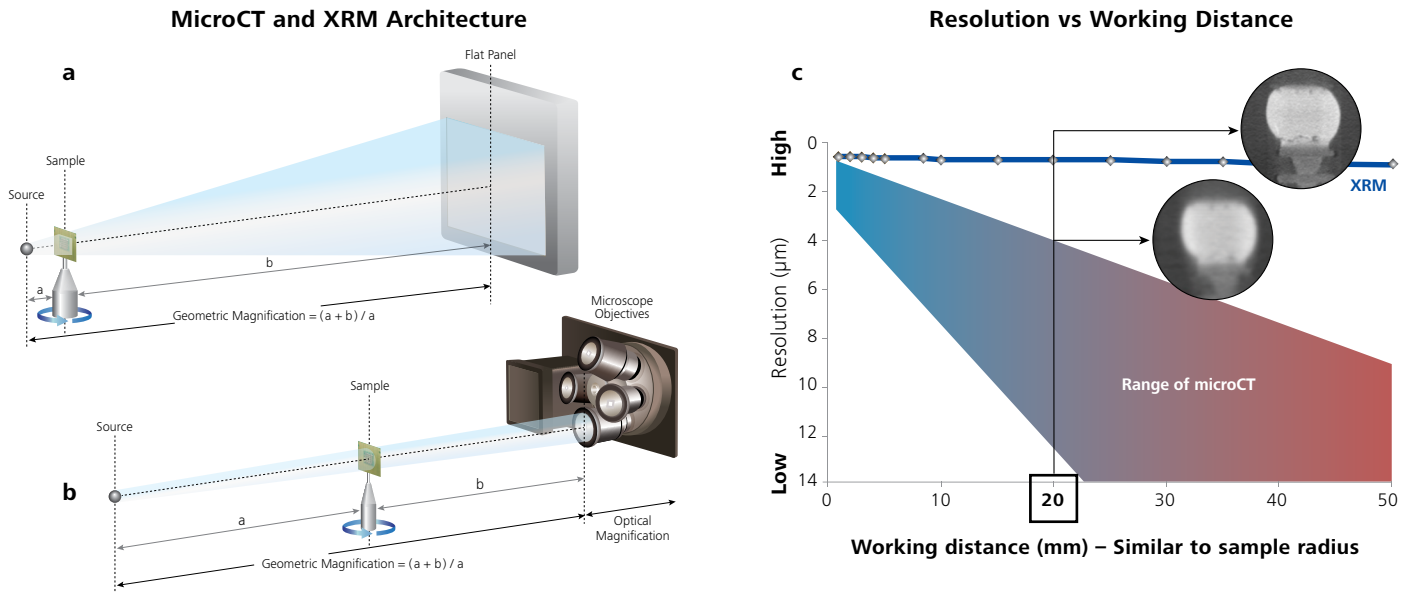

Figure 2 *a) The set-up for microCT imaging operates on principles of geometric magnification, b) 3D XRM implements optical magnification, c) XRM maintains high magnification at long working distances and high resolution for large samples.*

AI-Enabled 3D X-ray Microscopy

When 3D XRM emerged two decades ago it was a breakthrough method for non-destructive, high-resolution imaging of advanced packages, revealing details impossible to see in 2D X-ray projections (Figure 4). However, when imaging a region of interest (ROI) within a large sample at the highest resolution, 3D XRM throughput can be on the order of many hours. Additionally, like all microscopies, the high magnifications required for high resolution result in a small field of view. The combination of slow scan times and small field of view limits the volume of material that can be analyzed at high resolution. To address this, an artificial intelligence solution using deep learning high-resolution reconstruction algorithms (DLHRR) was recently introduced, enabling faster data acquisition, improved image quality, and faster overall FA workflows. It uses a convolutional neural network algorithm based on the "noise2noise" model [7], and a proprietary cost function and user-executed neural network training method using a small amount of data to train the neural network model. DLHRR enables scan time improvements by a factor of 4X to 10X across a broad array of sample types without sacrificing resolution or usability [8] and is available commercially as ZEISS DeepRecon Pro, a module for ZEISS X-ray microscopes.

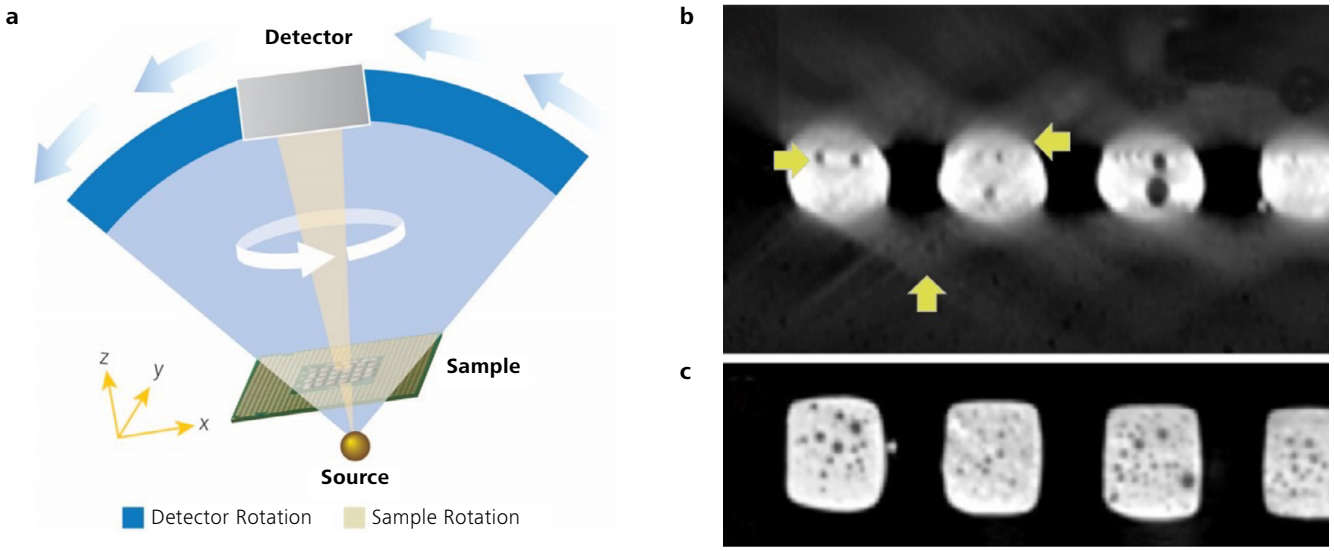

Figure 3 *a) Schematics of a 2.5D computed laminography setup, b) reconstructed XZ slice showing distorted structures and voids at the solder interfaces, and streak artifacts in the low-absorbing areas (arrows), c) reconstructed planar view XY.*

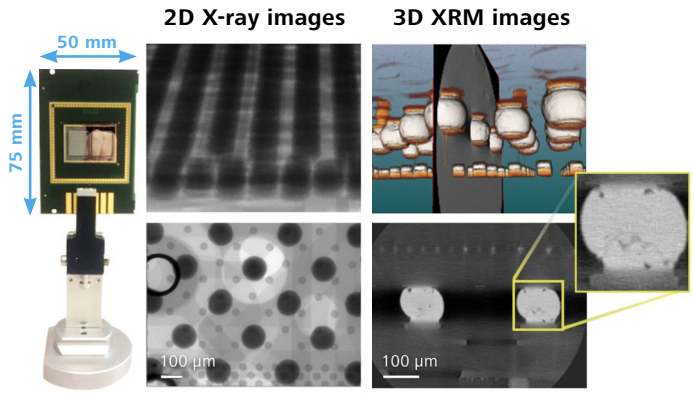

Figure 4 *3D XRM of a large 2.5D package reveals voids and cracks in flip chip bumps that are invisible in 2D X-ray images at any viewed angle.*

The speed gains come from the improved image contrast-to-noise ratios (CNR) that result from using DLHRR for 3D reconstruction instead of the common Feldkamp-Davis-Kreuss (FDK) or filtered back projection (FBP) algorithm, which uses a frequency domain filter. The high CNR enables a reduction in dwell time and/or the number of angular projections required for a high quality image (Figure 5a, to the right), and for semiconductor packages, the typical scan time improvement is 4X (Figure 6a).

To train the neural network model, a single XRM tomography data set is used. The trained network can be applied to other samplescontaining comparable X-ray attenuation and consistent scan parameters, including X-ray source and filter settings as well as magnification. Typically, no parameter tuning or customization by the operator is required. The training of a new network to address different scan settings or a new sample class takes about 3 hours, and the application of the network back to a reconstructed data set takes less than 5 minutes for a volume of 1000^3 voxels. This enables faster time to results for applications like construction analysis, FA and reliability studies where multiple similar parts must be scanned, and multi-site construction analysis, where multiple ROI in an individual sample are scanned with similar scan settings, such as for reverse engineering or fault isolation where stitching multiple fields of scan volumes is required. DLHRR is likely to benefit unique samples as well, due to the combination of faster scan speeds with relatively fast time for autonomous model training using an offline workstation. DLHRR can speed up high-resolution 3D XRM by using fewer X-ray projections to get results in a less time or can be used to improve the image quality by keeping scan time constant with a "full" projection data set. In some instances, both speed and better image quality are obtained simultaneously (Figure 6b and 6c). DLHRR's multisite stitching effectiveness was proven for a Bosch Sensortec accelerometer/gyroscope by creating a 3 x 3 array of nine fields of view, each covering a 4 mm x 4 mm area. The network model was trained using the FOV in the center of the array, and successfully applied to all eight others [9].

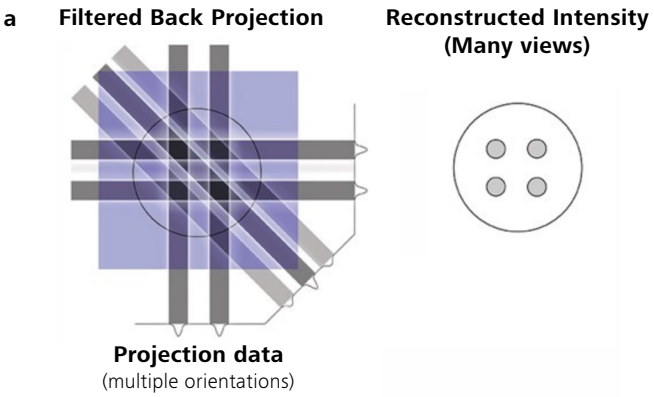

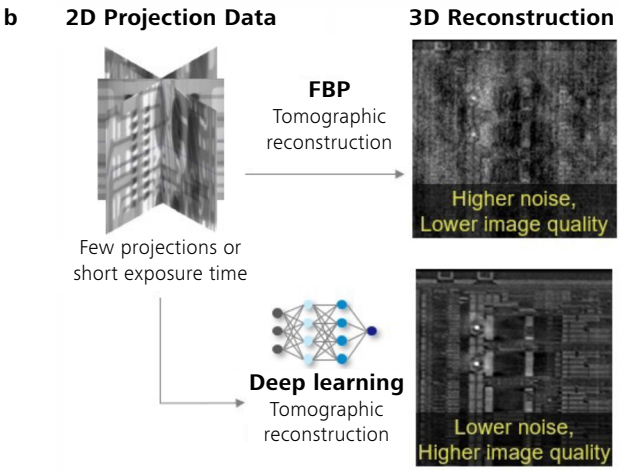

Figure 5 *a) In filtered back projection (FBP), projection data is filtered using a frequency domain filter, reducing image blurring. b) By integrating a pre-trained neural network between raw projection data and reconstructed data, high quality reconstructions can be achieved with low numbers of projections, and/or short exposures.*

The emergence of AI for 3D X-ray microscopy and package failure analysis enables more productive use of 3D XRM, higher FA success rates enabled by better image quality and improved CNR, and new applications that benefit from multiple-scan workflows on a single sample, or a single scan on multiple samples. Deep learning-based reconstruction decreases the effects of noise due to short exposure time and decreases the "streak" artifacts typically associated with sparse angular sampling. There are promising results for many types of samples, and the capability for a typical operator to easily train networks for new scan conditions or sample types will facilitate flexibility and responsiveness for a resource-constrained lab to adapt quickly to incoming requests. The application of AI to XRM makes the overall FA workflow faster, and it coincides with new innovations in FIB solutions addressing the physical failure analysis challenges of advanced packaging. Maximum benefit occurs when these advancements are combined into a synergistic workflow.

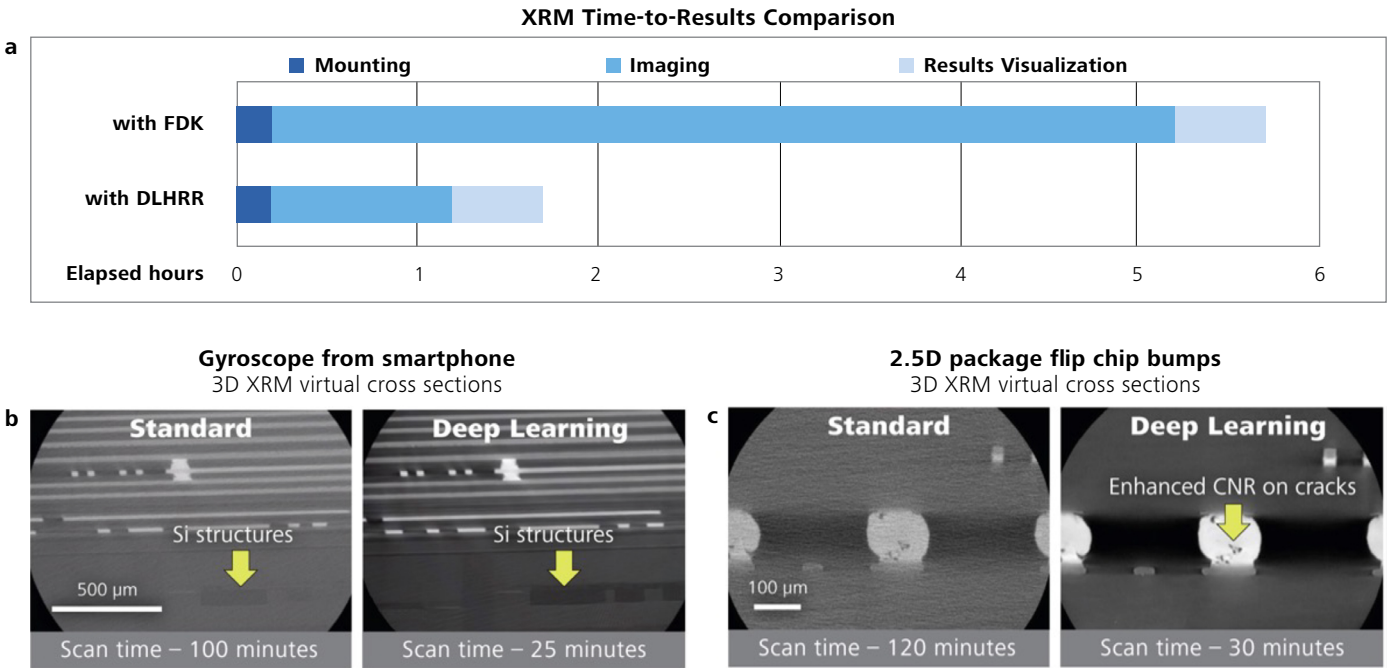

Figure 6 *a) DLHRR typically accelerates high-resolution 3D XRM imaging 4x versus using FDK reconstruction b) Image and scan time comparison for a gyroscope c) Image and scan time comparison for solder bumps in a large 2.5D large package.*

Advances in Focused Ion Beam Scanning Electron Microscopes

Drivers for New Cross Section Methods

According to the International Roadmap for Devices and Systems [10], near-term difficult packaging challenges include optimizing materials and processes for lower temperature assembly and for improved Cu resistance and reliability, while mitigating the impact of size effects in interconnect structures as they shrink. Meanwhile as packages become more complex, natural variations resulting from the packaging industry's historically wide process margins are emerging as a challenge for heterogenous integration, driving an increase in the volume of test die and learning cycles as failure modes are introduced through combinatorial package strategies [11]. This increased volume of test and learning cycles drives increasing pressure for fast and efficient analysis during development and later during production to maximize yields. Cross-sectional analysis is a common task in package construction evaluations and FA workflows. Cross sections allow one to view shapes and dimensions of interconnects, measure layer thicknesses, and check intermetallic quality, as well as study defects related to test, assembly and production process parameters, chip-package interactions, and thermomechanical stresses. Optically-guided cross sectioning of important package structures and features is becoming more difficult as 3D packaging implementing fine-pitch interconnect penetrates nearly every semiconductor business sector.

ROI are often deeply buried and with package interconnect pitches now crossing 1 µm, traditional mechanical cross sections are increasingly challenged to target features and accurately end-point to a desired sample plane with high success rates. Large-area and high-quality cross sections can be made using a BIB to fine polish mechanical cross sections, and it is possible to achieve a cross section through the full length of a 30 µm-diameter wirebond with application of best practices for such techniques [12]. However, the targeting accuracy limit for BIB is around 15 µm, which means it would be a challenge to consistently achieve cross sections in the center of today's 25 µm-diameter microbumps.

The milestone of 1 µm package interconnect pitch is driving the requirement for FIB-SEM analysis into the packaging world, ushering in a new cross section era mimicking that seen decades earlier for die-level semiconductor analysis. To extend the usefulness of FIB-SEM to package cross sections, a fs-laser has recently been integrated into the FIB-SEM. This enables rapid material removal on a scale of millimeters with micron levels of precision, followed by accurate fine polishing with nanometer levels of precision (Figure 7). Adopting an architecture where the laser is parallel to the e-beam, and laser processing occurs in a dedicated ablation chamber rather than in the high-vacuum imaging chamber, this "LaserFIB" is known commercially as ZEISS Crossbeam laser [13] and well suited for the shrinking structures defining this new era of packaging (Figure 8).

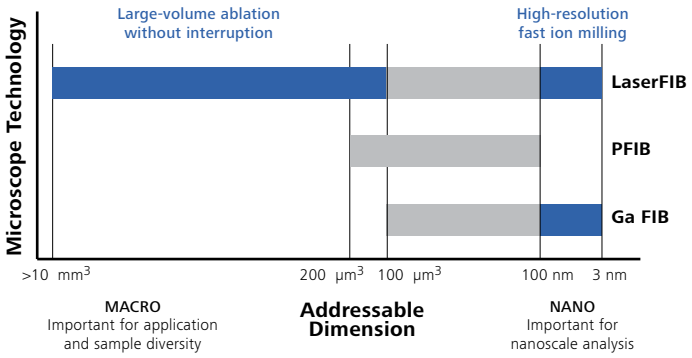

Figure 7 A fs-laser integrated into a Ga FIB-SEM instrument enables rapid targeted removal of millimeter material volumes, enabling nanoscale imaging and analysis over large areas and from deeply buried sample locations.

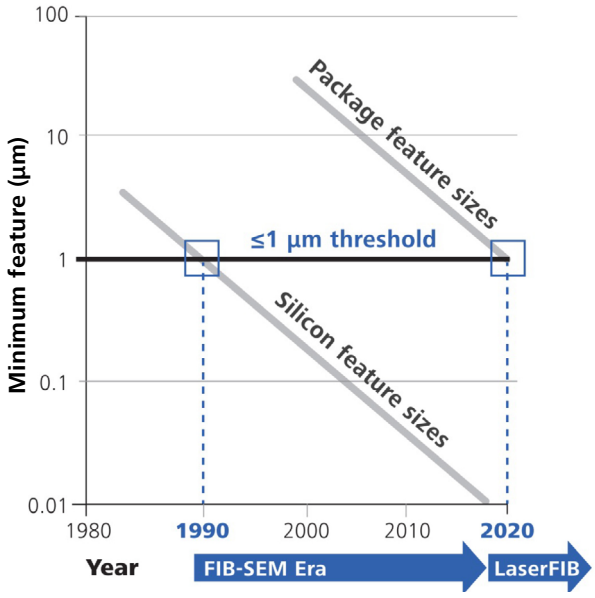

Figure 8 As die-level features hit 1 µm dimensions in 1990, FIB-SEM became a required cross-section technique. Packaging features are now crossing that same 1 µm threshold, driving FIB integration with fs-lasers to enable efficient and targeted millimeter-wide package cross sections for nanoscale analysis of buried features. Graph inspired by [18].

Laser-enabled Package Cross-Section Landscape

Standalone laser marking systems, even when using ps- or fs-lasers, lack integration and environmental conditions to efficiently target a small ROI by FIB after laser ablation. Commercial standalone laser systems implementing ultra-short-pulsed lasers specifically for sample preparation are effective for large-area preparation and package dissection but lack optimization for the fastest targeted microscopy preparation where ablation speed and sample quality are simultaneously important, since vacuum environments produce the best laser ablation and sample quality, in turn enabling efficiency for the subsequent FIB polishing steps. In contrast, the integrated LaserFIB approach has proven efficient and effective in correlative workflows with optical or XRM microscopy for a variety of research and industrial applications, including characterization of microbumps in a 3D package [14], development of automotive bumpers from recycled materials [15], correlative microscopy for rapid screening of Zr-containing particles for geochronology [16], and identification of random particles within an OLED display [17].

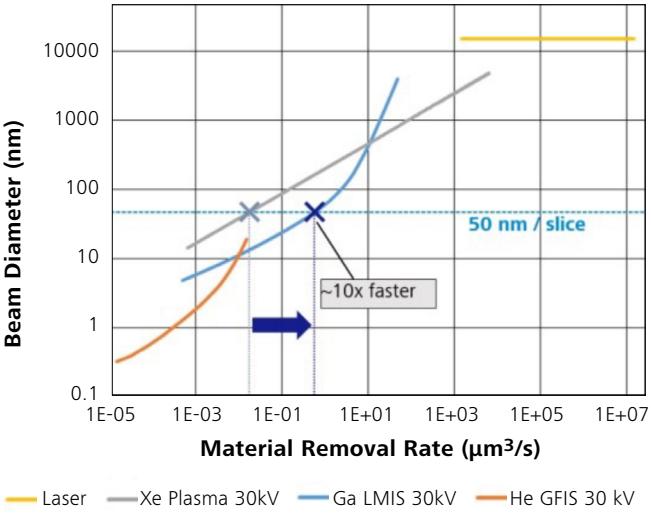

Figure 9 Beam diameters plotted as a function of material removal rates show that a Ga FIB is 10X faster than a PFIB at typical "thin slice" conditions required for fine ion milling.

The combination of fs-laser integrated within a FIB-SEM using Ga beam technology has proven highly efficient. Since the fs-laser can be targeted with high accuracy to within microns of its target, with minimal redeposition and a laser-affected zone <1 µm, the remaining volume of material after optimized laser ablation is suitable to polish by FIB. Polishing requires lower currents than large-volume ion milling, and Ga beams have 10X higher current densities than plasma beams at these low currents (Figure 9). The combination of targeted fs-laser ablation with fast Ga beam polishing is so effective that it can outperform a standalone laser plus PFIB combination. As Figure 10 shows for the cross section case of a targeted 500 µm-diameter solder ball, the LaserFIB cycle time was half that of the standalone laser plus PFIB combination, resulting in a doubling of FIB capacity and 2X faster time to results. While results may vary across different applications, it demonstrates the LaserFIB integration effectiveness.

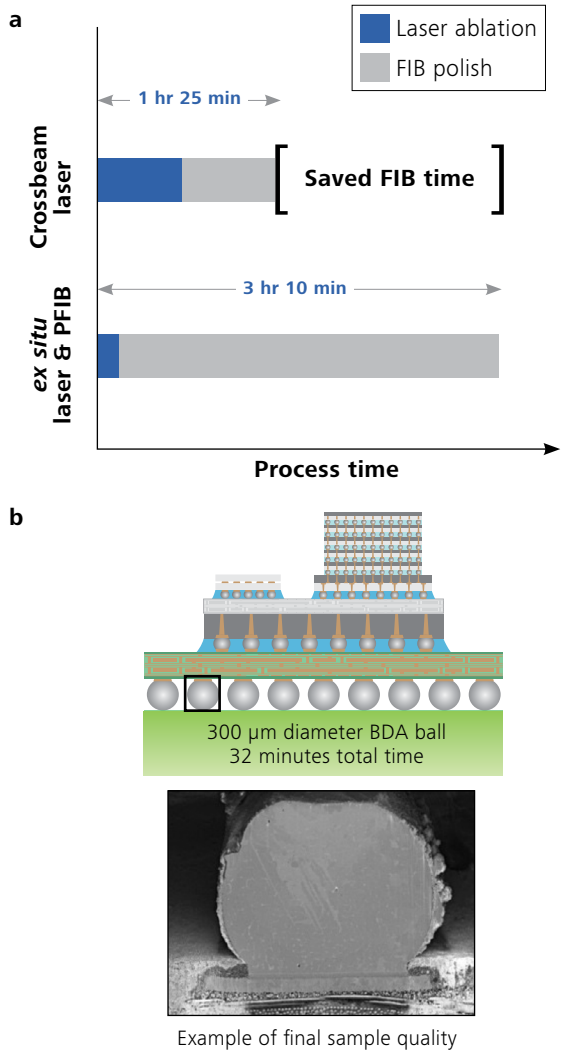

Figure 10 *a) A 500 µm-diameter solder ball was cross sectioned by the integrated LaserFIB and compared against a published workflow using a standalone laser and a PFIB [19]. The integrated LaserFIB saved FIB time and was 2X faster b) 32 minutes of LaserFIB preparation for a targeted 300 µm-diameter solder ball produces high sample quality.*

Due to the versatility enabled by a large laser scan area of 40 mm x 40 mm and an innovative cross-jet feature enabling the uninterrupted ablation of up to 10 cubic millimeters of material or more (depending on sample composition), the LaserFIB is suited for a broad range of different packaging and materials analysis applications, as indicated in Table 1 and Table 2.

Application	XRM correlation	Optical correlation
APU full cross section (15mm)		■
Buried Cu-pillar on GaAs die	■	
Bare wirebond ball bond		■
Seal ring on die		■
Solder ball cross section		■
SiC power module	■	
Unfilled TSV in GaN device		■
Trench-MOS with Cu clip	■	
Cu pillar solder bumps in IC	■	
Flip chip on board	■	
MEMS with metallic cap	■	
Multi-chip package	■	
Thermal interface material		■

Table 1 *Survey of correlative techniques in proven package FA LaserFIB cross section applications.*

Applications	Description	Suitability
2D laser cross sections	Remove volumes >> 2 mm^3 for large area imaging and analytics without breaking vacuum	■
Large-area EBSD	Prepare high-quality large surfaces for EBSD without ion polishing	■
TEM preparation	Efficiently and consistently prepare thin, site-specific, quality lamella for broadest range of materials including carbonaceous ones	■
Micromechanical test structures	Prepare large structures and large arrays in vacuum over a scan field of several centimeters,with unattended long running	■
Nanoscale XRM preparation	Create multiple sites (>0.5mm tall) anywhere from an intact large sample	■
Atom probe preparation	Prepare a large array of site-specific APT needles without using *in situ* lift-out	■
Correlated microscopy	Flexible, efficient sample-centric platform using features & fiducials on the sample for many modalities & length scales	■
TOF-SIMS	Air-free workflow to TOF-SIMS after laser cutting	■
No contamination	Main chamber kept free of laser-ablated debris	■
Avoidance of Ga-induced low-kV artifacts	Eliminate or minimize beam artifacts using milling, cryoFIB milling, or Ar polishing	■
Ga-free FIB polishing	Perform FIB milling without Ga	X
Fast viewing	Integrated SEM for efficient feedback of laser processing	■

Table 2 *LaserFIB suitability for different types of applications.*

The LaserFIB is well-suited as a site-specific cross section solution, where the ROI requires specificity better than 15 µm targeting accuracy, which is the limit for standard mechanical cross sectioning as discussed previously. Site specificity requires correlative microscopy, usually with X-ray or optical modalities. Computer aided design (CAD) layouts can also be helpful, but only 3D XRM reveals the true 3D location of buried objects. For the various applications listed in Table 1, slightly more than half involve buried features and require a 3D XRM correlative workflow to enable cross sectioning the designated site. Software solutions are available to aid the overlay of images of different modalities in the LaserFIB, including 3D XRM data. The laser spot's diameter is <15 µm, and with registration procedures, the laser's accuracy for targeting a surface feature can be better than 2 µm. The LaserFIB's Ga beam removes the excess material using live SEM imaging during FIB milling to achieve end-pointing in the targeted location, with accuracy better than 10 nm possible. The LaserFIB is also well-suited for tasks that have low targeting requirements, for example to prepare a sensitive interface or material that would fall apart using alternative methods. In general, laser ablation volumes should be kept in the range of 10 cubic millimeters or less, for reasons of time savings and ensuring uninterrupted laser operation.

Effective LaserFIB Workflows

As the technology moves into the field, new workflows are arising. A particularly effective LaserFIB workflow makes use of the fs-laser to create shallow "sample-centric" ruler-based surface fiducial marks for multimodal microscopy. The LaserFIB can laser scribe a T-shaped ruler to cover millimeters of area in less than a minute, with measurement divisions of 25 µm or more (Figure 11). The ruler is visible in optical, XRM, and SEM imaging modes, and adds efficiency to correlative workflows. In Figure 12 the ruler fiducials are used to guide the laser placement for site specific cross-sectioning of a targeted Cu pillar microbump in a smartphone package-on-package (POP). This example involved iterations of two-hour 3D XRM scans to aid process set-up and confirm target accuracy. In this case, the entire XRM to LaserFIB workflow took less than one day [17]. Figure 13 shows the steps of the workflow. The XRM scans are executed at steps A (for defect visualization) and E (to capture the fiducial marks by XRM). A third XRM scan (not shown) was performed right after laser ablation to confirm the proximity of the buried defect to the surface of the cut face. This was done as a precaution while developing the workflow and is an optional step.

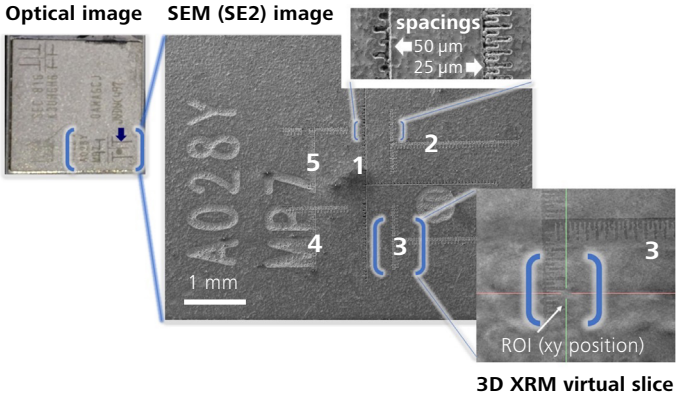

Figure 11 *Five shallow "T-shaped" ruler fiducials scribed onto the surface of a package-on-package sample are numbered for clarity. Ruler divisions are 25 and 50 µm (top image zoom). The XY position of the buried ROI relative to the fiducials is determined from a 3D XRM virtual slice at the sample's surface (right image zoom).*

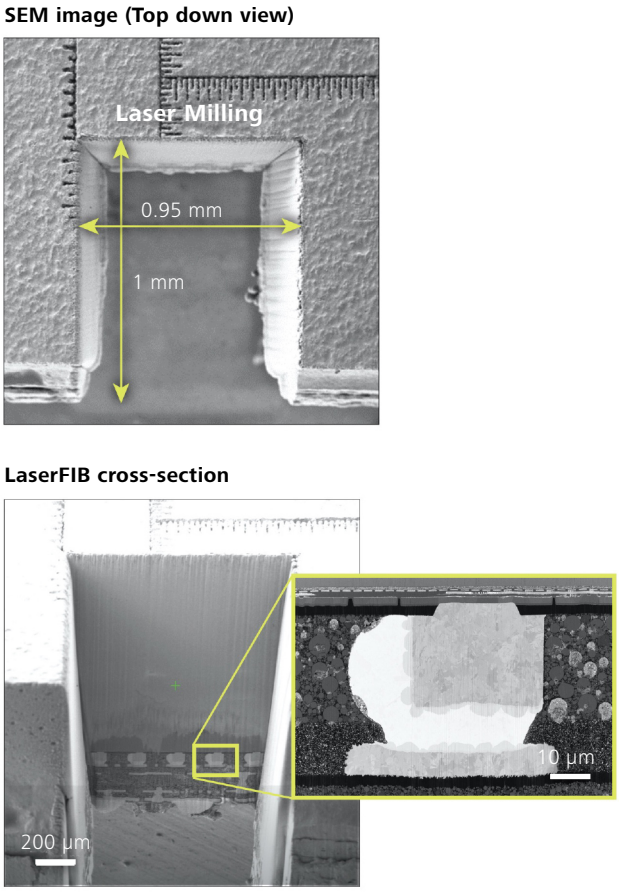

Figure 12 *A small Cu-pillar bump in a smartphone package-on-package (POP) is accurately targeted, cross sectioned and imaged with the aid of laser-made fiducials.*

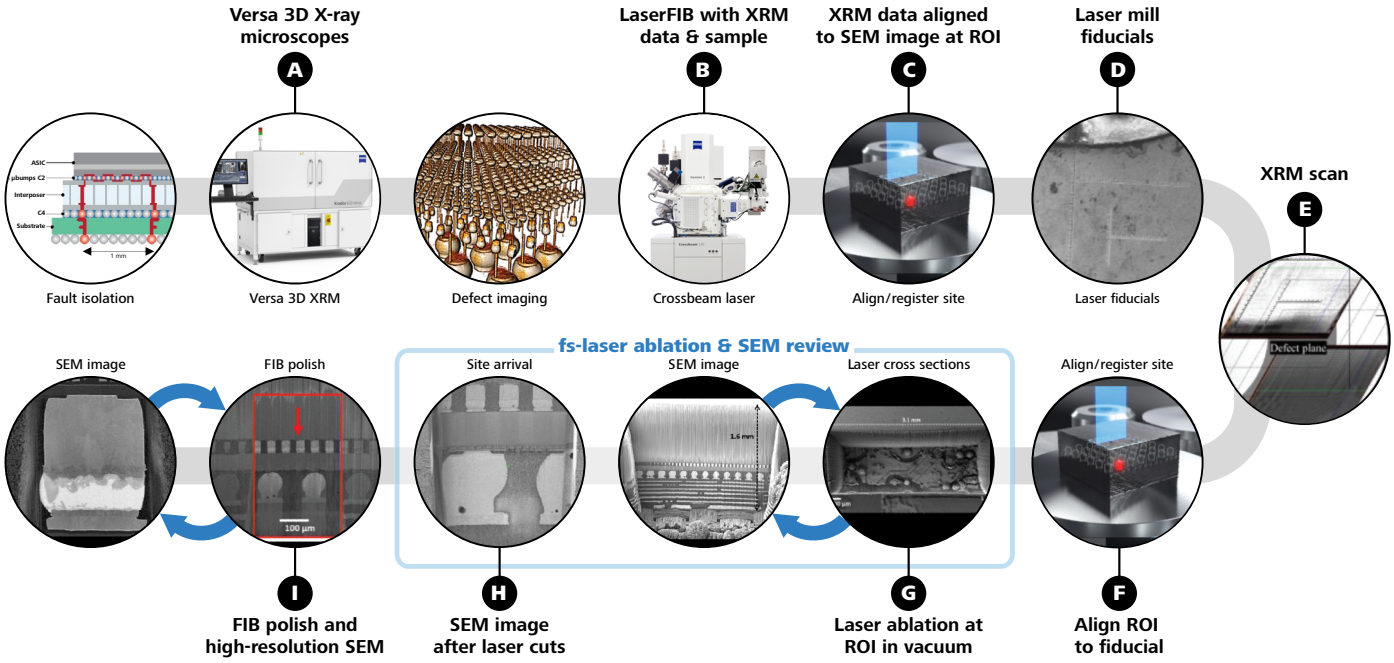

Figure 13 *Steps of a correlative XRM to LaserFIB workflow. Sample-centric "ruler" fiducials are created at step D, scanned in XRM, and then visualized in the LaserFIB to guide the targeted ablation. The rulers can also be created as the first step. Integration facilitates iterative cut and view cycles (solid box) for laser optimization and end-pointing.*

Summary

The inspection and analysis of 3D packages is becoming more difficult due to buried package interconnects that have higher I/O densities and finer pitches, the insufficiency of 2D analysis, and the increase in cycle time as the package complexity and volume of testing increase. Rapid and precise analysis of deeply buried structures is essential. Advancements in 3D X-ray microscopy and FIB-SEM microscopes offer significant speed improvements. In an AI-enabled approach to improve faster data acquisition, 3D XRM has incorporated deep learning algorithms. Meanwhile, the FIB-SEM has been integrated with a fs-laser, resulting in the LaserFIB, a new class of FIB-SEM instrument. As a result, 3D XRM data acquisition speeds can be increased by 4X and sometimes more than 10X, while the LaserFIB enables millimeters of material removal within minutes to hours, instead of the days required by conventional Ga or plasma FIB. With these new 3D XRM and FIB-SEM advancements combined into an optimized correlative workflow, it is possible to produce high-resolution microscopy images enabled by the FIB's submicron targeting precision and the fs-laser's rapid material removal, which provides access to deeply buried features with submicron laser-affected zones. These advancements enable multi-site sampling at practical timescales and extend the toolset for package development, failure analysis and reliability studies. This supports fast development of reliable next-generation package technology by enabling the combination of speed, site targeting, and end-pointing accuracy required to address increasingly complex devices with higher throughput and success rates.

Acknowledgments

The authors wish to thank the many people in the ZEISS demonstration centers around the world that developed the first applications with these new instruments, as well as ZEISS colleagues Stephan Hiller and Ravi Sanapala for being stalwart champions in guiding the new product developments.

References

[1] ASE Group, What is 2.5D? [Video], https://ase.aseglobal.com/en/technology/advanced_25dic (2022) Accessed on July 16, 2022 at https://coms.aseglobal.com/marcom/video/25d-ic at timestamp 1:20.

[2] A. Gupta, Z. Tao, D. Radisic, H. Mertens, O. V. Pedreira, S. Demuynck, J. Bömmels, K. Devriendt, N. Heylen, S. Wang, K. Kenis, L. Teugels, F. Sebaai, C. Lorant, N. Jourdan, B. Chan, S. Subramanian, F. Schleicher, A. Peter, N. Rassoul, Y. Siew, B. Briggs, D. Zhou, E. Rosseel, E. Capogreco, G. Mannaert, A. Sepúlveda, E. Dupuy, K. Vandersmissen, B. Chehab, G. Murdoch, E. Altamirano Sanchez, S. Biesemans, Z. Tőkei, E. D. Litta and N. Horiguchi, Buried power rail integration for CMOS scaling beyond the 3 nm node, SPIE (2022).

[3] H. S. P. Wong, K. Akarvardar, D. Antoniadis, J. Bokor, C. Hu, T.-J. King-Liu, S. Mitra, J. D. Plummer and S. Salahuddin, Proceedings of the IEEE, 108, 478 (2020).

[4] C. D. Hartfield, T. M. Moore and S. Brand, in Microelectronics Failure Analysis: Desk Reference, 7th ed., T. Gandhi Editor, ASM International (2019).

[5] B. A. J. Quesson, P. L. M. J. v. Neer, M. S. Tamer, K. Hatakeyama, M. H. v. Es, M. C. J. M. v. Riel and D. Piras, in Proc.SPIE (2022).

[6] A. Gu, M. Terada and A. Andreyev, A Brief Comparison of Computed Laminography versus 3D X-ray Microscopy for Electronics Failure Analysis, Carl Zeiss Microscopy GmbH [White Paper], (2022).

[7] J. Lehtinen, J. Munkberg, J. Hasselgren, S. Laine, T. Karras, M. Aittala and T. Aila, Noise2Noise: Learning Image Restoration without Clean Data, in Proceedings of the 35th International Conference on Machine Learning, D. Jennifer and K. Andreas Editors, p. 2965, PMLR, Proceedings of Machine Learning Research (2018).

[8] M. Andrew, R. Sanapala, A. Andreyev, H. Bale and C. Hartfield, Supercharging X-ray microscopy using advanced algorithms, in Microscopy and Analysis, Wiley Analytical Science (2020).

[9] A. Gu, A. Andreyev, M. Terada, B. Zee, S. Mohammad-Zulkifli and Y. Yang, in ISTFA 2021, p. 291 (2021).

[10] IEEE, The International Roadmap For Devices and Systems: 2021, [White Paper], (2021).

[11] E. Sperling, Variation Making Trouble In Advanced Packages, in Semiconductor Engineering, [White Paper], (2022).

[12] T. Rodgers, A. Gu, G. Johnson, M. Terada, V. Viswanathan, M. Phaneuf, J. de Fourestier, E. Ruttan, S. McCracken, S. Costello, A. M. Robinson, A. Gibson and A. Balfour, in ISTFA, p. in press (2022).

[13] B. Tordoff, C. Hartfield, A. J. Holwell, S. Hiller, M. Kaestner, S. Kelly, J. Lee, S. Müller, F. Perez-Willard, T. Volkenandt, R. White and T. Rodgers, Applied Microscopy, 50, 24 (2020).

[14] M. Kaestner, S. Mueller, T. Gregorich, C. Hartfield, C. Nolen and I. Schulmeyer, in CSTIC, China (2019).

[15] T. Schubert, R. Salzer, A. Albrecht, J. Schaufler and T. Bernthaler, Combined light-microscope – FIB/SEM failure analysis on automotive body parts, [White Paper], (2021).

[16] J.H. Li, Q.L. Li, L. Zhao, J.H. Zhang, X. Tang, L.X. Gu, Q. Guo, H.X. Ma, Q. Zhou, Y. Liu, P.Y. Liu, H. Qiu, G. Li, L. Gu, S. Guo, C.-L. Li, X.H. Li, F.Y. Wu and Y.X. Pan, Geoscience Frontiers, 13 (2022).

[17] V. Viswanathan, L. Jiao and C. Hartfield, in 2021 IEEE 23rd Electronics Packaging Technology Conference (EPTC), p. 80 (2021).

[18] R. Hollman, in Pan Pacific Microelectronics Symposium (2019).

[19] M. Tuček, R. Blando, R. Váňa, L. Hladík and J. V. Oboňa, in International Physics of Failure Analysis (IPFA), Singapore (2020).

Originally Published at 2021 IEEE 23rd Electronics Packaging Technology Conference (EPTC)

Developments in Advanced Packaging Failure Analysis using Correlated X-ray Microscopy and LaserFIB

Vignesh Viswanathan, Longan Jiao, Cheryl Hartfield
Carl Zeiss Pte Ltd 80 Bendemeer Road, #10-01, Singapore 339949

Abstract

The evolution of packaging architecture with increasing density and scaling of features is resulting in large footprints to accommodate more components and functions that are integral in the heterogeneous integration roadmap and the More-than-Moore era. These developments pose new challenges in failure analysis and process characterization and drive need for advances in analysis tools, techniques, and development of novel workflows. In this work, we discuss the advances in two classes of techniques that have gained traction in the advanced packaging industry, 3D X-ray microscopy (XRM) and laser-integrated focused ion beam scanning electron microscopes (FIB-SEM) for sample preparation. While the laser integration in the FIB-SEM workflows has improved cross-section preparation throughput, precise targeting for site specific analysis of buried features requires the correlation with a complementary technique to provide sub-surface information. The use of 3D XRM to guide laser-integrated FIB-SEM analysis presents several advantages to address this challenge. In this work, we describe a novel workflow using 3D XRM and fs-laser integrated in a FIB-SEM (also called a LaserFIB) to precisely target and deliver results at high throughput. This represents a significant development in addressing the challenges of advanced package failure analysis.

Introduction

Advanced packaging developments for improved system performance and increased functionality in integrated circuits are driving the More-than-Moore era. Diverse 2.5/3D architectures with increasing density and shrinking interconnect dimensions and pitches, in combination with novel materials, has created complex challenges in package characterization and failure analysis (FA). These trends mandate new capabilities to enable fast development of package processes and rapid analysis of buried high density features.

For physical analysis, non-destructive characterization at the micron scale using submicron 3D XRM for imaging and a LaserFIB for high throughput cross-section preparation and imaging has been explored previously and is becoming widely adopted [1-8]. X-ray computed tomography is an important non-destructive characterization technique in the package FA workflow. With the increasing footprints of over 100 x 100 mm^2 area and complex 2.5D and 3D architectures, submicron resolution for such large packages is challenging to achieve using conventional projection optics. The Resolution at a Distance (RaaD) capability and objective coupled scintillators in the ZEISS Xradia Versa X-ray microscope enables high-resolution imaging of large packages without compromising resolution [1-3]. With further developments in the recently introduced machine learning based reconstruction algorithms, improvements in both image quality and up to 4X increase in throughput can be achieved [9-11]. These improvements enable workflows using multiple 3D XRM scans to accurately localize defects and correlate with sample preparation techniques such as FIB-SEM.

Non-destructive analysis with 3D XRM is usually followed by physical analysis using mechanical or FIB cross-sections. Compared to the conventional Ga+ FIB, plasma FIB technology provides higher throughput for preparation of large cross-sections and volumes that are <0.5 mm^3 [12]. The addition of laser processing in the workflow has increased the throughput by multiple folds for larger volume removal and to access deeply buried structures using both standalone laser systems and integrated laser FIB systems as reported previously [4-8]. Adoption of pulsed femtosecond laser ablation results in a small laser-affected zone with minimal material damage even at high material removal rates. A parallel FIB-SEM and fs laser architecture enables laser milling in a separate chamber to promote cleanliness of the main FIB-SEM chamber for ultra high-resolution imaging and analysis. This integrated dual chamber architecture promotes ablation volumes as large as >10 mm^3 in lidded packages, stacked multi-dies and intact large packages.

To achieve high success rates in the failure analysis of site-specific buried defects, correlation with fault isolation techniques and 3D XRM is essential when preparing cross-sectional samples so that localized defects have the desired orientation for optimal viewing of the defect or process variations [12-14]. Here, the LaserFIB excels and offers higher precision and speed than standalone systems. Quick 3D XRM scans to verify the sample status at different stages of LaserFIB work promotes an ability to make adjustments to improve the targeting accuracy. To enable the workflow, precise registration of the coordinate systems between the X-ray tomography data and the LaserFIB is necessary to target subsurface sample features that are not visible by SEM or optical microscopy due to lack of fiducials or patterned features on the sample surface close to the region of interest. In this work, we address this challenge and present a novel 3D XRM and LaserFIB workflow that improves the laser targeting accuracy by using laser-patterned fiducial markers and Atlas 5 software to correlate 3D XRM and LaserFIB images, enabling precise buried feature targeting and high throughput LaserFIB sample preparation guided by 3D X-ray microscopy images.

Experimental Methods and Results

The workflow developed for precise targeting of sub-surface features is presented as a series of sequential steps in Figure 1.

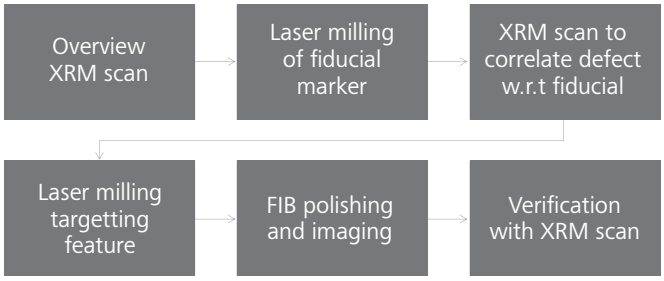

Figure 1 *Workflow overview.*

An overview XRM scan of the region of interest and high resolution scans, if required for visualization of the defect, are acquired. The sample surface near the deeply buried defect is then patterned with fiducial markers using the fs-laser. The sample is scanned again using the XRM to measure the relative position of the defect with respect to the fiducials on the sample surface. The coordinates mapping now provides the precise location for the laser milling pattern placement on the sample surface with respect to the fiducial markers for targeted sample preparation.

After the laser milling, the cross-section is further polished with the Ga FIB to remove the redeposition and small laser-affected zone, and to position the feature of interest in the desired final plane. The XRM tomography can be performed again at any point to verify the targeting accuracy.

The demonstration of this workflow is performed using ZEISS Xradia 520 Versa X-ray microscope and a ZEISS Crossbeam 350 laser FIB-SEM. The sample is an OLED display of a broken mobile phone. A small section at the top corner of the display, where the probability of defects is high, is cut and mounted on a pin for the XRM scan. For XRM-correlated LaserFIB work, the pin with the sample is mounted on a sample stub that mounts on the LaserFIB sample holder as shown in Figure 2b.

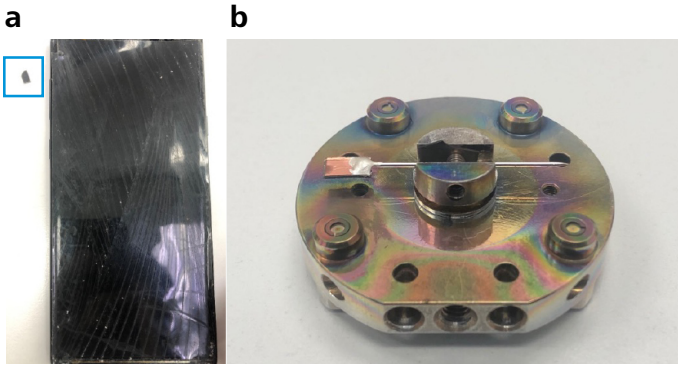

Figure 2 *(a) Small section of display from broken mobile phone is prepared and mounted on a pin for XRM investigation. (b) Pin is mounted on a stub on the LaserFIB sample holder to enable correlated LaserFIB processing.*

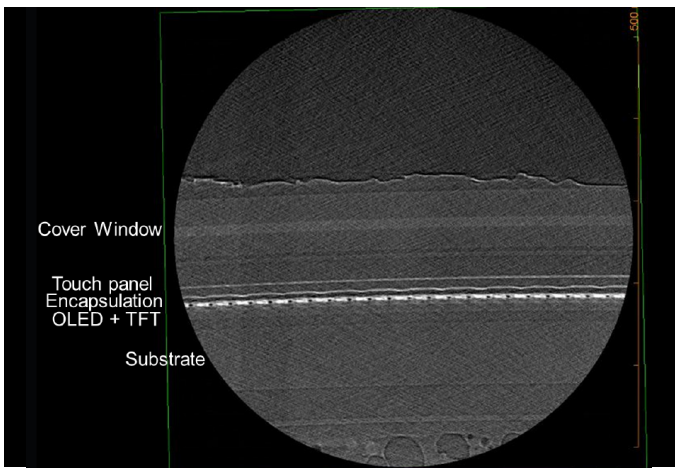

Figure 3 *XRM virtual cross-section of the OLED display with various layers highlighted. The strong absorption contrast in low Z materials allows clear identification of the different layers of polymeric and organic materials.*

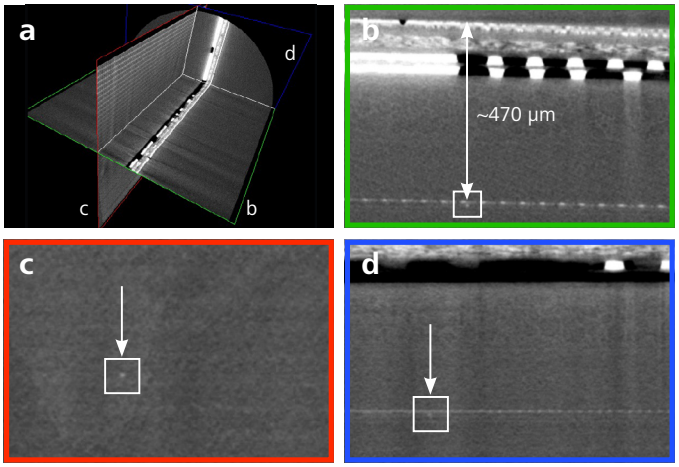

Figure 4 *(a) 3D reconstructed volume highlighting the virtual cross sections in three orthogonal planes indicated by (b) green, (c) red and (d) blue. The defect particle is highlighted by the green, red and blue arrows in the respective planes.*

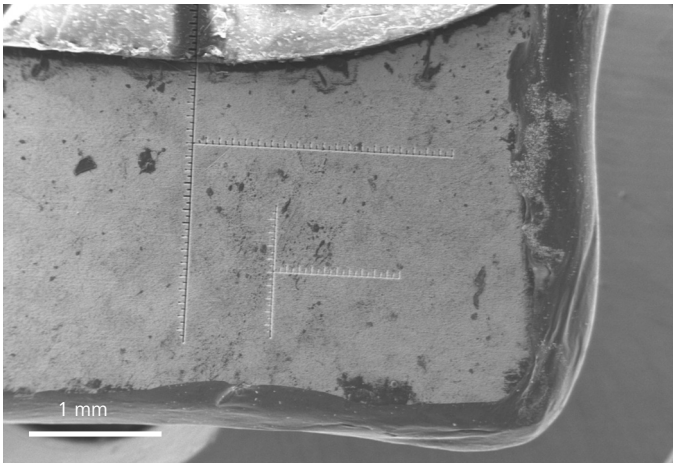

Figure 5 *SEM image of the double ruler grid patterned using the fs laser with a major scale of 100 µm and minor scale of 50 µm over 1 mm x 1 mm for the smaller ruler and 2 mm x 2.7 mm for the larger ruler.*

A low-resolution overview XRM scan of the sectioned sample is acquired in 2 hours with a resolution of 3 µm/voxel. The virtual cross-section shows the various layers in the display with good contrast of the organic and polymeric layers, indicating the mechanical sample preparation has caused minimum damage with most of the layers intact, Figure 3. Further analysis of the data indicates a particle defect is embedded inside a layer near the OLED and TFT circuitry, as seen in the virtual cross-sections at different planes as highlighted in Figure 4. The particle is estimated to be less than 10 µm in diameter and at a depth of 470 µm from the package substrate as indicated in Figure 4b. A higher resolution scan was not necessary since the particle is visible. However, there are no unique features to reference the position of the particle in the plane c shown in Figure 4c. Cross-section analysis of this defect particle requires an accurate determination of the particle position with reference to surface features near its location, enabling optimal placement of the FIB or laser milling patterns. Since the defect particle size is smaller than the 15 µm diameter of the fs-laser, the positioning information is critical.

To address these challenges, a fiducial marker that resembles a double grid is patterned on the surface of the sample using the ZEISS Crossbeam 350 laser FIB-SEM. The smaller grid is 1 mm x 1 mm long and larger grid is 2 mm x 2.7 mm. Both have a major spacing of 100 µm and minor spacing of 50 µm. The laser milling takes less than 10 seconds to pattern the fiducial, which can be customized to various grid spacings and orientations depending on the target feature. The pattern is immediately imaged with the electron column in the LaserFIB to check the laser milling fidelity and overall position of the marker, Figure 5. Optimization of the laser milling parameters for different or new materials can also be performed in this step to optimize the quality, calibrate milling rates, and achieve depth control.

Subsequently the sample is scanned with the XRM at the same region with the same parameters as the earlier scan. The 3D XRM data is imported into the LaserFIB's Atlas 5 software, and then using Atlas 5, 3D XRM virtual cross-sections at the plane of the defect are projected onto the plane with the fiducial markers to determine the position of the defect with respect to the grid, Figure 6.

With the defect coordinate locked-in relative to the marker grids, the milling patterns are positioned accordingly. The placement of the mill patterns position considers the 15 µm laser spot size and side wall taper created by the laser beam profile and is well calibrated to target the defect precisely.

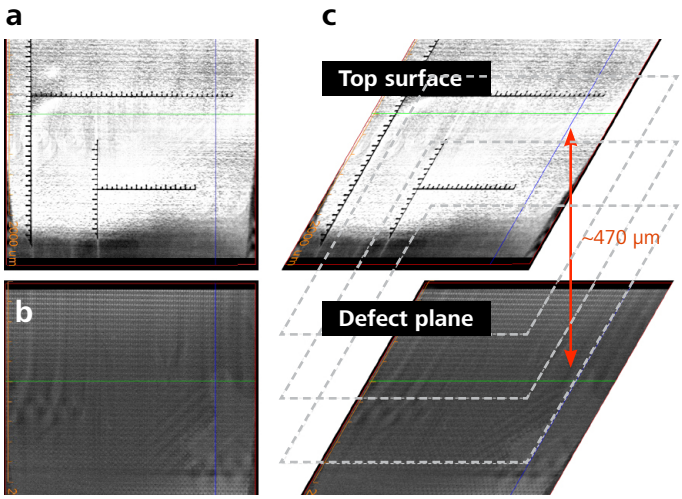

Figure 6 *XRM virtual cross-section of the (a) top surface with fiducial markers and (b) defect with the position marked by the crosshair that is projected in the vertical plane to reference with the marker as shown in (c). The defect is ~470 µm below the surface and its position can be mapped to the grid.*

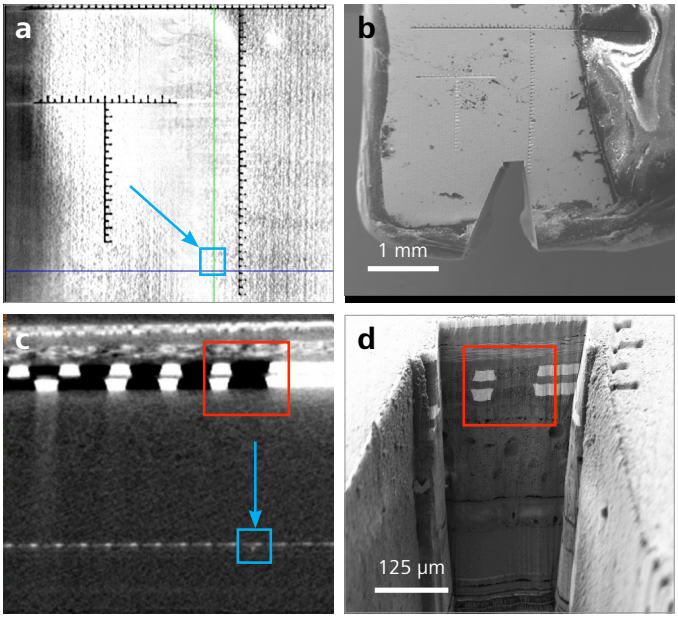

Figure 7 *(a,c) XRM virtual cross-section with the arrow pointing to the position of the defect can be compared with the (b) top down and (d) cross-section SEM view of the laser milled patterns indicating accurate targeting of the defect particle. The metal layers in the substrate as highlighted by the box in (c, d) also provide a reference to the defect position.*

The fs-laser milling is performed within 10 minutes in two steps: 1) a coarse laser mill at 15% of the maximum power to remove the bulk material, and 2) a fine laser mill at 8% power to polish the cross-section face and minimize damage to beam sensitive materials. The coarse mill volume with the trapezoid shape is about 0.85 mm^2 x 0.6 mm and the fine polish volume is 0.03 x 0.25 x 0.6 mm^3. Figure 7b shows the top-down view highlighting the position of the laser milled patterns with respect to the grid markers, and Figure 7d shows the cross-section view immediately after the laser milling. Comparing the XRM image in Figure 7a with the crosshairs highlighting the defect position, it can be observed that the laser milling is on target. The copper metal lines in the substrate can also provide an indication of the targeting accuracy as highlighted by the box in Figure 7c and d.

The particle is not clearly visible immediately after the laser milling due to redeposition and requires FIB polishing to clean up the surface. A gallium FIB polish at 65 nA for 20 minutes is performed to remove the redeposition and to target and expose the defective particle. The particle is visible immediately as the redeposition is cleared, although additional FIB polishing is required to remove the curtains and acquire a clear cross section. The final cross-section image with the in-column backscatter electron signal shows the defect in bright contrast indicating a metallic particle about 6.5 µm in diameter between the OLED and encapsulation layers, Figure 8.

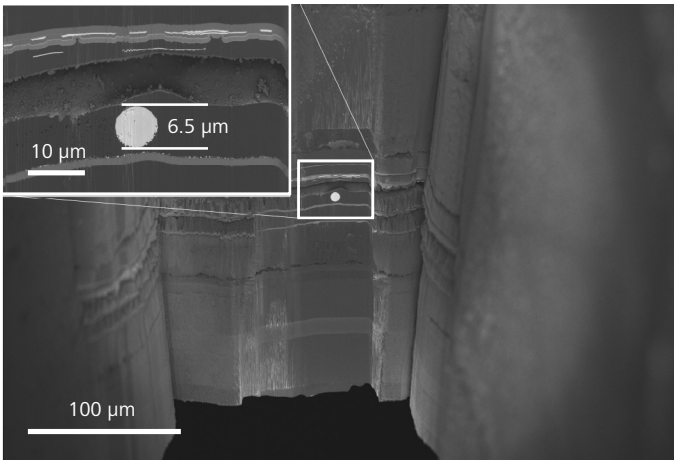

Figure 8 *Cross-section image of the metallic defect with higher magnification inset with particle diameter measuring 6.5 µm.*

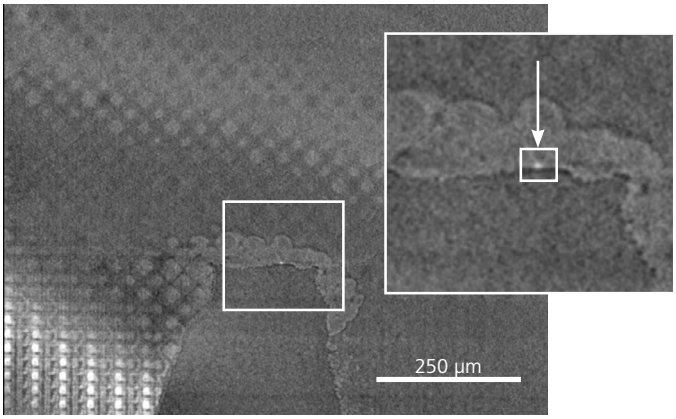

Figure 9 *XRM virtual cross-section after laser and FIB milling indicating the particle was targeted precisely. The inset shows the particle highlighted by the arrow that is targeted in the preparation.*

The targeting is verified with another XRM scan of the cross-sectioned sample. The virtual XRM cross section shows the particle cross-section perfectly aligned with the milled pattern, Figure 9.

Discussion

The workflow detailed in the earlier section demonstrates high precision in targeting deeply buried defects during failure analysis. The precision and minimum feature size that can be targeted is limited by two factors, the resolution of the X-ray microscope and the laser placement accuracy, which is on the order of 1-2 µm. In light of various fs-laser beam placement considerations including the laser spot size of <15 µm, the redeposition layer thickness, and the submicron laser affected zone, this work shows that this workflow for targeting deeply buried features of interest can routinely achieve laser targeting accuracy of better than 5 µm.

Continued developments to improve the laser accuracy will push the targeting accuracy towards the submicron scale, which further supports the requirements of 3D packaging technologies. However, additional understanding of the laser interactions with the new materials used in advanced packaging technologies would be necessary to achieve higher precision and targeting with this approach.

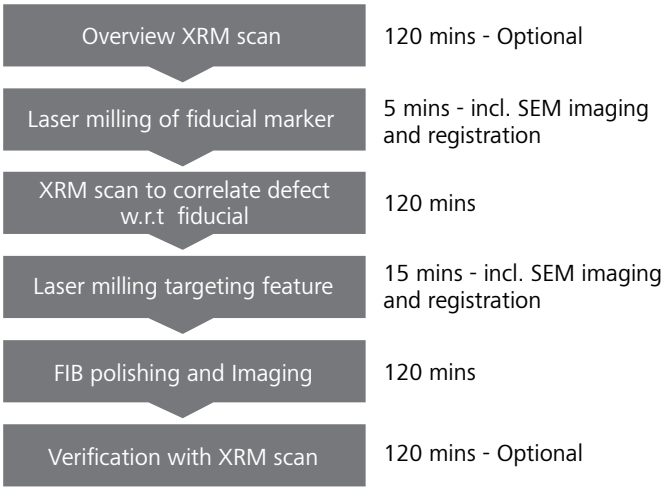

Figure 10 *Workflow overview with time taken for each step. Some of the 3D XRM steps are optional, depending on the fault isolation methods employed, which can significantly improve the time to result.*

Considering the throughput and time to result, we see that the workflow takes around 6:40 hours with the most time taken during the 3D XRM data acquisition, Figure 10. In most failure analysis, the fault isolation is performed using other techniques such as thermal emission, scanning acoustic microscopy, laser scanning confocal microscopy and other techniques.

In such cases, step 1 in the workflow could be skipped to directly pattern the sample surface with the laser and execute 3D XRM scans to visualize the defect and correlate the fiducials on the surface. The final verification step with 3D XRM can also be omitted from the analysis in most cases. This lowers the time to results to about 2.5 hours in this case, which represents a significant improvement in both throughput and accuracy in site specific failure analysis of defects. Although there are multiple 3D XRM scans performed, the recently available advanced reconstruction techniques based on machine learning algorithms can significantly reduce the scan times while preserving the image quality to gain throughput in this workflow [10-11].

Conclusions

A novel correlative workflow using LaserFIB and 3D XRM techniques is presented for targeted cross-section preparation of deeply buried subsurface defects and features. The case study presented is a particle defect found in the OLED display from a used mobile phone. The 520 Versa 3D XRM was used to scan and identify the defect and correlate with surface features patterned on the sample using the Crossbeam 350 fs-Laser FIB-SEM for precise targeting and sample preparation. The large area cross sections were prepared using the fs-laser followed by Ga+ FIB polishing in 35 minutes. The particle size is 6.5 µm in diameter and buried about 470 µm from the package substrate surface close to the OLED and TFT layers. The entire process from defect isolation until the cross-section preparation and analysis of the defect is completed in less than 5 hours highlighting the throughput and precision capabilities of this streamlined workflow to meet the demands and success requirements in the failure analysis of advanced packages.

Acknowledgments

The authors would like to acknowledge the support from ZEISS Microscopy Customer Centre Shanghai in providing the microscopes and tools used to developthis workflow and would also like to thank Henry Cai for the samples donated for this case study.

References

1] Sylvester Y., Hunter L., Johnson B. and Estrada R., "3D X-ray microscopy: A near-SEM non-destructive imaging technology used in the development of 3D IC packaging," 2013 IEEE International 3D Systems Integration Conference (3DIC), 2013, pp. 1-7.

2] Zulkifli S. M., Zee B., Qiu W. and Gu A., "High-res 3D X-ray microscopy for non-destructive failure analysis of chip-to-chip micro-bump interconnects in stacked die packages," 2017 IEEE 24th International Symposium on the Physical and Failure Analysis of Integrated Circuits (IPFA), 2017, pp. 1-5.

3] Bhuvanendran Nair Gourikutty S., et al., "Defect Localization in Through-Si-Interposer Based 2.5D ICs," 2020 IEEE 70th Electronic Components and Technology Conference (ECTC), 2020, pp. 1180-1185.

4] Stegmann H., Dömer H., Cai H., Rosenkranz R. and Zschech E., "Efficient target preparation by combining laser ablation and FIB milling in a single tool," 2011 Semiconductor Conference Dresden, 2011, pp. 1-4.

5] Randolph, S. J., Filevich, J., Botman, A., Gannon, R., Rue, C., & Straw, M. "In situ femtosecond pulse laser ablation for large volume 3D analysis in scanning electron microscope systems" Journal of Vacuum Science & Technology B, Vol. 36, No. 6 (2018), 06JB01.

6] Tuček M., Blando R., Váňa R., Hladík L. and Oboňa J. V., "Speeding up large-scale failure analysis of semiconductor devices by laser ablation," 2020 IEEE International Symposium on the Physical and Failure Analysis of Integrated Circuits (IPFA), 2020, pp. 1-3.

7] Johnson G. M., Hartfield C., Mueller S. and Kaestner M., "New physical analysis capability for counterfeit electronics and reverse engineering," 2020 IEEE Physical Assurance and Inspection of Electronics (PAINE), 2020, pp. 1-5,

8] Tordoff B., Hartfield, C., Holwell, A.J. et al. "The LaserFIB: new application opportunities combining a high-performance FIB-SEM with femtosecond laser processing in an integrated second chamber," Appl. Microsc. Vol. 50, No. 24 (2020)

9] Andrew, M., and Hornberger, B. "Benchmarking of Machine Learning and Conventional Image Segmentation Techniques on 3D X-ray Microscopy Data". Microscopy and Microanalysis, 24(S2), (2018) pp.118-119

10] Gu A., Andreyev A., Terada M., Zee B., Zulfikli S.M. and Yang Y. "CASE STUDIES - DEVICE ANALYSIS: Accelerate Your 3D X-ray Failure Analysis by Deep Learning High Resolution Reconstruction", International Symposium for Testing and Failure Analysis (ISTFA), 2021

11] Andrew M., Sanapala R., Hartfield C. and Atkinson-Mora J. " Advanced Reconstruction Technologies for Semiconductor Advanced Packaging", Technical Note, https://zeiss.widen.net/s/7scxlhbhm8/en_wp_3d-xray-art-for-semiconductor

12] Hartfield C., Kaestner M., Mueller S., Atkinson-Mora J. and Schullmeyer I., "A new approach for rapid analysis of buried 2.5/3D package structures", Chip Scale Review Vol. 24, No. 3 (2020) pp. 39-42.

13] Kaestner M., Mueller S., Gregorich T., Hartfield C., Nolan C., Schulmeyer I., "Novel workflow for high-resolution imaging of structures in advanced 3D and fan-out packages", China Semiconductor Technology International Conference (CSTIC) (IEEE, Shanghai, 2019), pp. 1–3.

14] Leslie N., Lai B., Lee H., Lee M., Kang C.H., Patakova Z., Zelenka F., and Varslot T., "Addressing Failures in Advanced Packaging Through a Correlative Workflow" International Symposium for Testing and Failure Analysis (ISTFA), 2020, pp. 17-19.

Originally Published at ICSJ 2022: Proceedings from 11th IEEE Components, Packaging and Manufacturing Technology (CPMT) Symposium Japan (ICSJ)

Targeted Sample Preparation and Analysis of Advanced Packaging using Correlated X-ray Microscopy and LaserFIB

Vignesh Viswanathan
Research Microscopy Solutions, Carl Zeiss Pte Ltd, Singapore, Singapore

Takehide Oda, Etsuo Maeda, Chisato Yamamoto
Research Microscopy Solutions, Carl Zeiss Co., Ltd., Tokyo, Japan

Longan Jiao
Research Microscopy Solutions, Carl Zeiss (Shanghai) Co., Ltd., Shanghai, China

Abstract

X-ray microscopy and femtosecond (fs) laser integrated FIB-SEM are combined in a workflow to guide precise and targeted sample preparation to enable functional testing and fault isolation without damaging the package and IC.

Introduction

Emerging technologies such as AI, 5G, IoT, wearables, cloud, computing, and autonomous vehicles hold great promise for improvement and transformation of human lives globally. In today's More-than-Moore era, advanced packaging has emerged as a critical enabler for these next generation of electronic devices. System level performance improvements through heterogeneous integration has added more functionality while improving the cost-performance gaps. Developments in various materials, processes, and architectures for 2.5D and 3D packaging has enabled high density interconnects with shrinking dimensions and pitch which is essential for continued scaling in performance and integration of various devices at lower costs.

As the complexity of electronic packages continues to increase, so do the challenges in characterization during process development and failure analysis (FA). Traditionally, FA workflow in IC packaging begins with the electrical and functional testing of the device followed by incoming optical and 2D X-ray inspection. Subsequent fault isolation using multiple tools and techniques have become necessary starting with curve tracing, TDR, high resolution, non-destructive imaging using SAM, X-ray CT, and IR imaging followed by physical analysis using mechanical and focused ion beam (FIB)-based cross-sectioning for visualizing and characterization of defects, Figure 1. [1]

Once the fault isolation is completed and a failure site has been localized, high-resolution imaging techniques such as 3D X-ray microscopy (XRM) can visualize defects and guide sample preparation for physical analysis to disclose defects for root cause investigation [2, 3]. However, the region of interest (ROI) may be several hundreds of microns (µm) or millimeter (mm) deep into the package which requires removal of large volume of material with high accuracy in the microns or better range. Conventional techniques such as mechanical cross-section enable large cross-section preparation but are slow and have limited accuracy. FIB using liquid metal ion source or plasma ion source is very precise and effective in preparing cross-sections in the hundreds of microns cubic volume which would still need long preparation times to access deep structures (hours to days). Laser ablation using ultra-fast pulsed lasers have been adopted as stand-alone and integrated into FIB systems which allows large volume removal (mm^3) at high throughput (minutes to hours) [4-7].

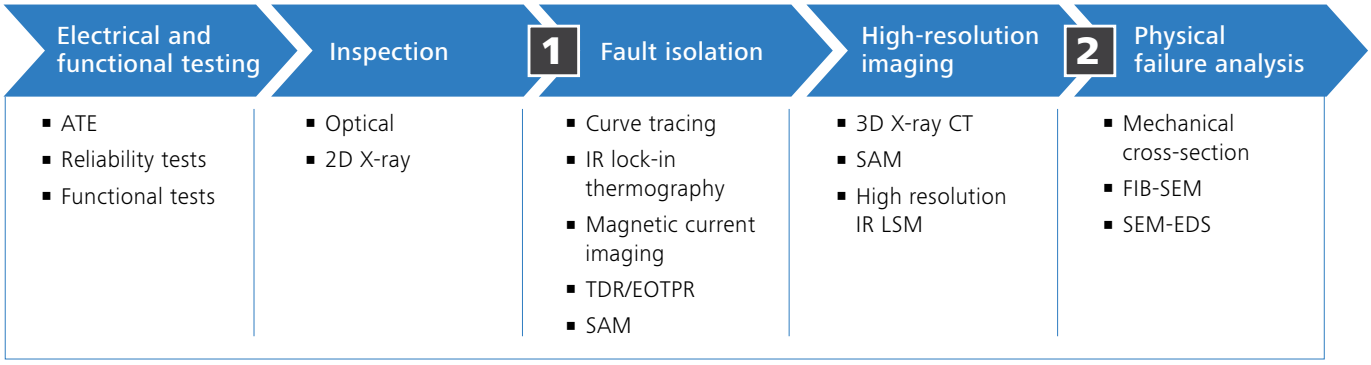

Figure 1 *IC package FA workflow with sample preparation steps at 1 and 2*

For targeting sub-surface and buried features, an XRM-guided workflow for sample preparation through integrated laserFIBs has already demonstrated high precision and high throughput sample preparation in 2.5D packaging and display [8-11]. Besides large volume removal, the ability to access deeply buried structures with high precision can also be used to selectively sever electrical wires and connections to simplify and isolate complex circuitry during fault isolation.

In advanced packages with high IO and complex interconnect structures, localization of tiny defects by electrical curve tracing, TDR, or lock-in thermography can be challenging. Finding these failures in complex packages such as system-in-package, multi- stack dies and package-on-package devices with several functional components can be quite time consuming. Deduction by elimination would require disconnecting or breaking the electrical connectivity in parts of the circuitry without affecting any other component which can be a challenge. This would require a precise and selective technique to break the interconnects and wires while retaining all other functionalities of the device.

In this work, we apply a workflow combining a non-destructive 3D X-ray microscopy that guides the sample preparation using a FIB integrated with an fs laser with high precision for fault isolation in 3D packages.

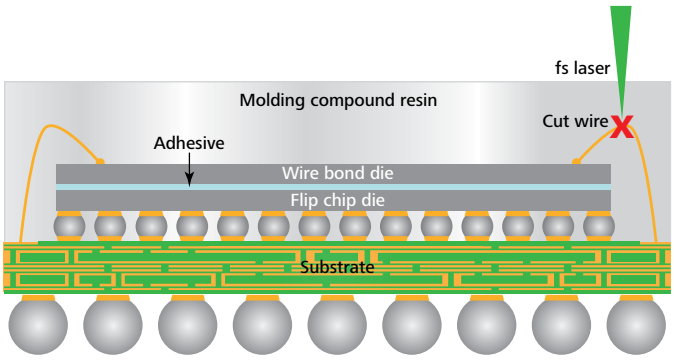

Figure 2 *Schematic illustrating how wire bond can be cut to isolate functions from the top die during functional testing and fault isolation*

Methods

A. Sample Preparation

For the demonstration of this workflow, we extracted a base band modem IC from the motherboard of a mobile phone, which is a 3D package consisting of one flip-chip die (baseband processor) connected to the substrate through solder bumps and another die (memory and/or analog) with wire bonds. Upon preliminary inspection, no damage to the internal structures was observed.

B. Workflow

In 3D packages, electrical connections going to the different modules may have complex circuitry that could lead to challenging fault isolation routines to identify the failure sites. In such 3D packaging, it would require deactivating certain features or parts of the circuit to isolate some components and determine failure sites with higher accuracy. The ability to selectively break an interconnect or wire without damaging the chip for functional testing can be achieved if they are accessible either through the molding compound or through other protective packaging materials as highlighted in Figure 2.

The workflow combines two techniques, a high-resolution non-destructive 3D X-ray microscopy and an fs laser integrated FIB-SEM. In this work, we utilize ZEISS 620 Xradia Versa and ZEISS Crossbeam laser 550 to perform the analysis. Figure 3 illustrates the process and steps involved. The sample is scanned at low resolution to obtain an overview of the entire package and interconnect structure to check for defects or anomalies. This information may be available from other fault isolation techniques or known data and may be skipped. Once the region of interest (ROI) is identified, this must be referenced to a unique feature that is visible and accessible for imaging either by SEM or optical methods on the surface. Hence, the top surface above the ROI is marked to add fiducials for easy reference to the sub-surface feature. The package is scanned again using the X-ray microscope at sufficient resolution to capture both ROI and the surface fiducials to localize the ROI with respect to the surface fiducials.

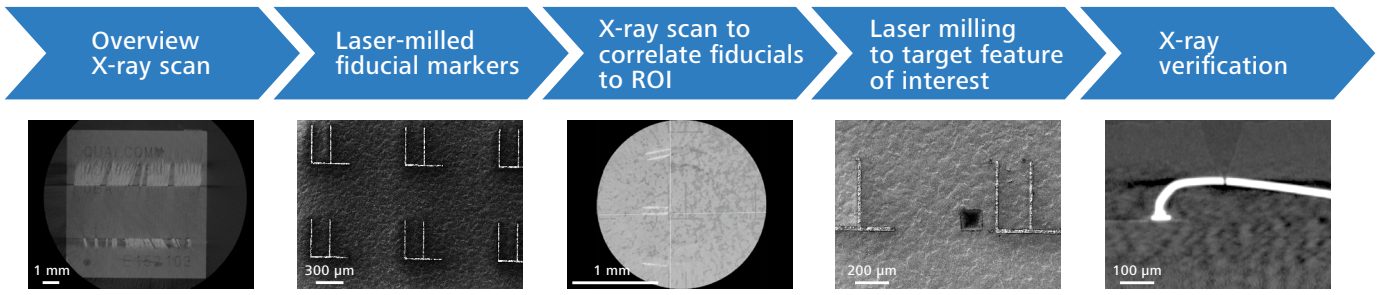

Figure 3 *Sample preparation workflow process using 3D X-ray guided laser milling of interconnects for fault isolation*

Subsequently, the fs laser is used to perform a precise fine cut on the desired wire or interconnect to isolate features or parts of the circuitry. The sample is again checked using the X-ray to determine if the precise cutting is sufficient or successful for further fault isolation.

In this example we demonstrate that the 20 µm wide wire that is 150 µm deep can be precisely cut with the laser without decapsulating or damaging any part of the die and other interconnects or neighboring wires. To improve the laser milling accuracy, a calibration step is performed to determine the parameters for accurate positioning and laser milling depth. Once the calibration is performed, thelaser parameters can be replicated on additional wires or on other samples made of similar materials. The results are presented in the next section.

Results

The first experiment is performed to determine the optimal milling parameters, Figure 4. The second experiment is performed targeting a single wire to demonstrate precision and replication of the milling parameters on other sites, Figure 5. The overview X-ray scan is acquired in 28 minutes at 100kV, 14W and 12 µm/voxel. The low-resolution fast scan is sufficient to observe the internal structure of the devices and layout of the interconnects and wires. The sample is mounted on a carbon stub which allows transfer of the sample between the XRM and LaserFIB. Subsequently, the sample is transferred to the LaserFIB to generate fiducial markers on the top right. The Crossbeam laser 550 operates with a separate chamber for laser milling and has micron scale accuracy with a registration process between the SEM and laser. The laser milling is performed at 4W with a pulse frequency of 10 KHz and milling time is 1 second. The fiducial markers are 20 µm wide and over 1.2 mm x 1.2 mm. The sample is scanned again with the XRM at higher resolution at 2 µm/voxel at 100kV and 14W in 2 hours.

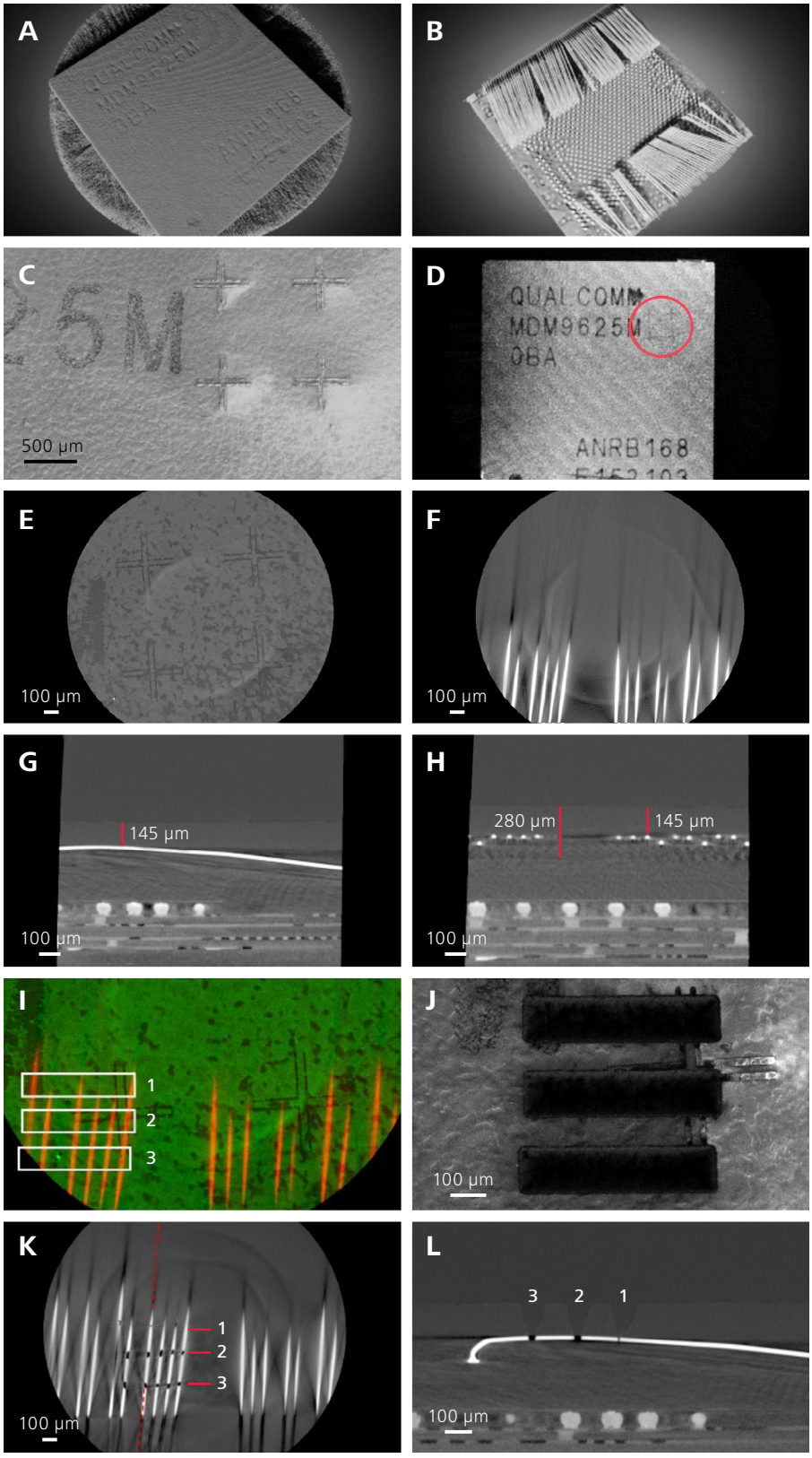

Figure 4 *A) Overview X-ray scan of chip showing top molding compound surface and B) internal wires and flip chip bumps. C) SEM image after laser marking of fiducials. D) XRM overview showing position of fiducials highlighted by red circle. E) Higher magnification XRM scan virtual cross-section of the fiducials and F) underlying wires. G) and H) Distance of the wires and chip from the top surface is measured to be 145 µm and 280 µm respectively. I) Top surface (in green) with laser fiducuals is overlayed with wires (in orange) and the position of laser milling test patterns 1,2 and 3 with varying doses are shown. J) SEM image after laser milling. K) XRM scan showing virtual cross-section on top of the wire and L) virtual cross-section view of wires cut corresponding to the 3.*

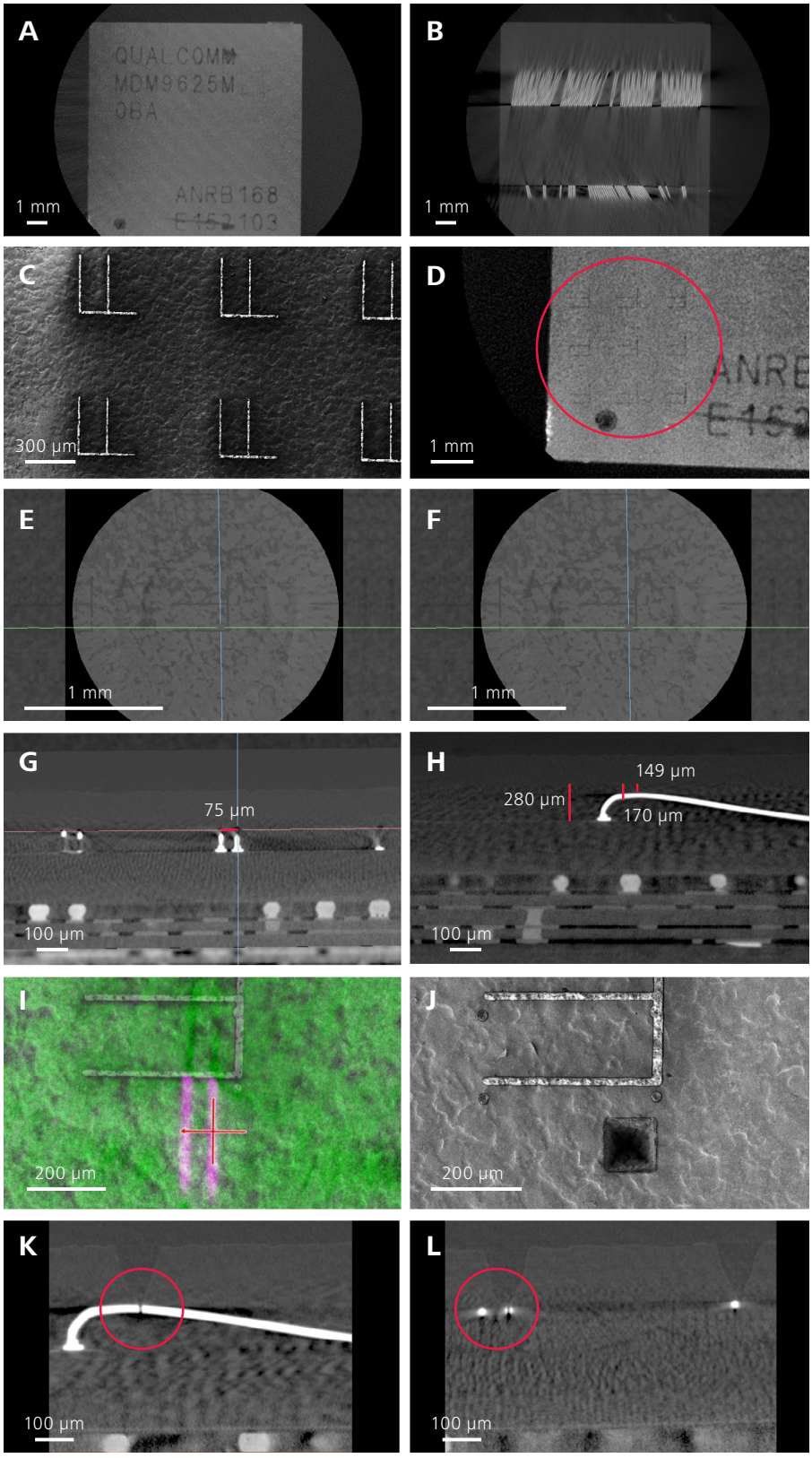

Figure 5 *A) Overview X-ray scan of chip showing top molding compound surface and B) internal wires and flip chip bumps. C) SEM image after laser marking of fiducials. D) XRM overview showing position of fiducials. E) Higher magnification XRM scan virtual cross-section of fiducials and F) underlying wires. G) The distance of wire from neighboring wire and H) distance of wire from top surface and distance of chip from the top is measured to be 149 µm and 280 µm respectively. I) top surface (in green) with laser fiducuals is overlayed with the wires (in pink) and the position of laser milling is highlighted by the crosshair. J) SEM image after laser milling 100 x 100 µm square targeting 150 µm deep wire. K) XRM scan showing virtual side view of cut wire while L) maintaining neighboring wire.*

Now both the ROI and fiducial markers are captured. The position of the wires with respect to the laser milled surface fiducial markers can be determined by overlaying the two virtual cross-sections. The wire is 145 µm below the surface and has a diameter of about 20 µm. The die is 280 µm below the surface giving a clearance of about 115 µm from the bottom of the wire. Since the material information is not known, the laser milling parameters are to be optimized with a dose test such that the milling only cuts the wire and does not penetrate deeper to damage the die. A series of rectangles (labelled 1, 2 and 3) 100 µm x 100 µm is milled at 4W with a frequency of 10 KHz and speed of 20 mm/sec while varying additional parameters to control the milling depth to determine the optimal conditions for the laser milling. The milling pattern cuts multiple wires providing several data points to check for repeatability and local variations in the materials due to fillers or additional components. The milling takes less than 20 seconds to complete. The sample is then scanned again in the XRM at 2 µm/voxel at 100kV and 14W in 2 hours to check the depth of the laser cuts. It can be observed that the dose in rectangle 1 is insufficient to cut the wire reliably while the dose in rectangles 2 and 3 cut the wires and do not damage the die below. The optimal dose is chosen to be dose 2.

The same workflow is now followed to target a single wire in another area of the chip as shown in Figure 5. Previous X-ray overview scans provide low resolution position information to laser mill surface fiducial marks on the lower left corner of the chip. Laser milling of fiducials follow earlier recipe and are completed in less than 1 second. Higher resolution X-ray scan at 2 µm/voxel is required to obtain accurate positioning of the target wire. The wire is about 150 µm from the top surface and the nearest wire is at a pitch of 75 µm. The overlay of the X-ray image with the fiducials and wires are aligned with the SEM image to provide a precise location of the wire, Figure 5I.

Now a 100 µm x 100 µm rectangle is positioned precisely and milled with the laser following the earlier recipe. The milling is completed within 20 seconds. The final X-ray scan verifies that the laser cut precisely targets the wire of interest and doesn't damage the neighboring wire or the die below indicating the workflow can be employed for precise and targeted sample preparation.

Discussion

In this work, the recipe is repeatable at different locations within the same sample and for similar packages using the same molding compound materials. However, the variations arising due to the presence of filler materials and other additives are not thoroughly studied and would need further optimization. The gaussian profile of the laser beam introduces a side wall taper of close to 15 degrees which adds requirements on the minimum opening area at the top surface to completely cut the wire and this depends on the depth of the interconnect from the surface. The entire workflow takes 5 hours and can be completed in 6-8 hours including data reconstruction and preparation time in between steps. Further functional testing of the chip is required to validate the proposed method and is part of the future work.

Conclusion

A novel correlative workflow using LaserFIB and 3D XRM techniques is presented for targeted sample preparation for fault isolation in 3D BGA packages consisting of wire bonds and flip chip devices. The case study presented targets an interconnect wire connecting the top die in the 3D package to isolate part of the circuit / device for functional testing and fault isolation. The 620 Versa 3D XRM was used to scan and identify the interconnects and features and correlate with surface features patterned on the sample using the Crossbeam 550 fs-Laser FIB-SEM for precise targeting and sample preparation. The wire was cut precisely without damaging neighboring wires or the die while retaining most of the package for further testing. The entire process from feature identification until the wire milling and isolation of the circuit is completed in 8 hours highlighting the throughput and precision capabilities of this streamlined workflow which can open new capabilities in the fault isolation and failure analysis of advanced packages.

Acknowledgement

The authors would like to acknowledge the support from ZEISS Microscopy Customer Centre Tokyo in providing the microscopes and tools used to develop this workflow.

References

[1] Pacheco, M., Wang, Z., Skoglund, L., Liu, Y., Medina, A., Raman, A., Dias, R., Goyal, D., and Ramanathan, S., "Advanced Fault Isolation and Failure Analysis Techniques for Future Package Technologies." Intel Technology Journal, 9(4) 2005.

[2] Sylvester, Y., Hunter, L., Johnson, B. and Estrada, R., "3D X-ray microscopy: A near-SEM non-destructive imaging technology used in the development of 3D IC packaging," 2013 IEEE International 3D Systems Integration Conference (3DIC), 2013, pp. 1-7.

[3] Nair Gourikutty S.B, Chow, Y. M., Alton, J., Umralkar, R.B., Bai, H., Chua, K.K., Bhattacharya, S., "Defect Localization in Through-Si-Interposer Based 2.5D ICs," 2020 IEEE 70th Electronic Components and Technology Conference (ECTC), 2020, pp. 1180-1185.

[4] Stegmann, H., Dömer, H., Cai, H., Rosenkranz, R. and Zschech, E., "Efficient target preparation by combining laser ablation and FIB milling in a single tool," 2011 Semiconductor Conference Dresden, 2011, pp. 1-4.

[5] Randolph, S. J., Filevich, J., Botman, A., Gannon, R., Rue, C., & Straw, M. "In situ femtosecond pulse laser ablation for large volume 3D analysis in scanning electron microscope systems" Journal of Vacuum Science & Technology B, Vol. 36, No. 6 (2018), 06JB01.

[6] Tuček, M., Blando, R., Váňa, R., Hladík, L. and Oboňa, J. V., "Speeding up large-scale failure analysis of semiconductor devices by laser ablation," 2020 IEEE International Symposium on the Physical and Failure Analysis of Integrated Circuits (IPFA), 2020, pp. 1-3.

[7] Tordoff, B., Hartfield, C., Holwell, A.J. et al. "The LaserFIB: new application opportunities combining a high-performance FIB-SEM with femtosecond laser processing in an integrated second chamber," *Appl. Microsc.* Vol. 50, No. 24 (2020)

[8] Hartfield, C., Kaestner, M., Mueller, S., Atkinson-Mora, J. and Schullmeyer, I., "A new approach for rapid analysis of buried 2.5/3D package structures", Chip Scale Review Vol. 24, No. 3 (2020) pp. 39-42.

[9] Kaestner, M., Mueller, S., Gregorich, T., Hartfield, C., Nolan, C., Schulmeyer, I., "Novel workflow for high-resolution imaging of structures in advanced 3D and fan-out packages", China Semiconductor Technology International Conference (CSTIC) (IEEE, Shanghai, 2019), pp. 1–3.

[10] Leslie, N., Lai, B., Lee, H., Lee, M., Kang, C.H., Patakova, Z., Zelenka, F., and Varslot, T., "Addressing Failures in Advanced Packaging Through a Correlative Workflow" International Symposium for Testing and Failure Analysis (ISTFA), 2020, pp. 17-19.

[11] Viswanathan, V., Jiao, L. and Hartfield, C., "Developments in Advanced Packaging Failure Analysis using Correlated X-ray Microscopy and LaserFIB", 2021 IEEE 23rd Electronics Packaging Technology Conference (EPTC), 2021, pp. 80-84.

Originally Published at ISTFA 2022: Proceedings from the 48th International Symposium for Testing and Failure Analysis Conference

A Correlative Microscopy Workflow For Nanoscale Failure Analysis and Characterization of Advanced Electronics Packages

Thomas Rodgers, Allen Gu, Greg Johnson, Masako Terada, Nathaniel Cohan, Vignesh Viswanathan
Carl Zeiss Microscopy GmbH, Carl-Zeiss Strasse 22, 73447 Oberkochen, Germany

Michael W. Phaneuf, Joachim de Fourestier, Ethan Ruttan
Fibics Inc., 1431 Merivale Rd #100, Ottawa, ON K2E 0B9, Canada

Stewart McCracken, Suzanne Costello, Aidan M Robinson, Andrew Gibson, Alan Balfour
Materials Consultancy Services Limited, Centre House, Midlothian Innovation Centre, Roslin, Midlothian, EH25 9RE, United Kingdom

Abstract

Microscopic imaging and characterization of semiconductor devices and material properties often begin with a sample preparation step. A variety of sample preparation methods such as mechanical lapping and broad ion beam (BIB) milling have been widely used in physical failure analysis (FPA) workflows, allowing internal defects to be analyzed with high-resolution scanning electron microscopy (SEM). However, these traditional methods become less effective for more complicated semiconductor devices, because the cross-sectioning accuracy and reliability do not satisfy the need to inspect nanometer scale structures. Recent trends on multi-chip stacking and heterogenous integration exacerbate the ineffectiveness. Additionally, the surface prepared by these methods are not sufficient for high-resolution imaging, often resulting in distorted sample information. In this work, we report a novel correlative workflow to improve the cross-sectioning accuracy and generate distortion-free surface for SEM analysis. Several semiconductor samples were imaged with 3D X-ray microscopy (XRM) in a non-destructive manner, yielding volumetric data for users to visualize and navigate at submicron accuracy in three dimensions. With the XRM data to serve as 3D maps of true package structures, the possibility to miss or destroy the fault regions is largely eliminated in PFA workflows. In addition to the correlative workflow, we will also demonstrate a proprietary micromachining process which is capable of preparing deformation-free surfaces for SEM analysis.

Introduction

As semiconductor package architectures become more complex, the schemes of heterogeneous integration provide greater complexity in dimensions, density, and delicacy of IC interconnects. The diagnosis methods of encapsulated structures and failures are under increasing demands. One challenge is to isolate and pinpoint fault regions with sufficient accuracy during the PFA process.

Because typical modern ICs are made of a variety of materials with different coefficients of thermal expansion (CTE), warpages exist ubiquitously in die, package, and PCB levels, resulting in significant positional shifts of the structures respective to IC designs. If the original design is used to guide cross-section, it may yield wrong surfaces, possibly losing defects or regions of interest permanently. The capability to acquire true 3D reconstruction of failure locations becomes crucial for the success of root cause analysis. Although the conventional mechanical lapping and BIB milling are effective to remove materials from large areas, it is not accurate because there is limited control at endpoint. Modern advanced packages are often made of various materials in silicon, metals, and organic polymers with length scales ranging from millimeters to nanometers. This dynamic provides additional challenges to the existing sample preparation and PFA workflows.

3D X-ray tomography has become an essential technique for construction and failure analysis of semiconductor packages [1-4]. Its non-destructive nature and high-resolution imaging capability make it an ideal tool to reconstruct package structures with high resolution. With the assistance of acquired 3D XRM datasets, analysts can virtually navigate through an entire package volume to identify specific regions of the interest and characterize failures. This makes the subsequent cross-sections more effective than xconventional polishing. Recently, we have demonstrated that the integration of laser ablation with focused ion beam (FIB) techniques for fine polishing has enabled rapid preparation of site-specific cross-sections with extremely high precision [5-6]. In this paper, we report a three-step PFA process dedicated to preparing SEM surface with high accuracy and pristine quality. Firstly, a semiconductor package is imaged with high-resolution 3D XRM, and regions of interest are defined at submicron accuracy. Secondly, using the acquired 3D X-ray data, a proprietary sample cross-sectioning process Perfect Edge [7] follows to generate accurate and distortion-free surfaces. Thirdly, the prepared surface is imaged and analyzed with FE-SEM.

Results

SiP Wire Bonds

A commercially available ADAQ23875 system-in-package (SiP) device was purchased using a standard commercial channel. The sample was overstressed with excessive current provided by a Keithley probe station. The test stopped when 100X decrease in current was observed in I-V curves. The sample then was imaged by 3D X-ray microscopy at 10 µm/voxel resolution to capture full field of view (FOV) of the package. 120 kV X-ray energy was used to image this medium density sample. A high-resolution image at 1.5 µm/voxel was acquired. Figure 1 shows the 3D color-rendering image and examples of reconstructed virtual slices.

The XRM data was processed using analysis workflows within ORS Dragonfly to "digitally" remove encapsulating packaging material and reveal the internal components of the SiP, including the gold wire bonds, ICs, passive components, and the underlying PCB substrate. In Figure 2, specific electric networks of interest with the suspicion of partial wire opening (associated with excessive resistance) are labeled on the planar views of the XRM images. The flexibility of 3D digital data manipulation makes it easy to visualize the internal structures at any orientation.

Having selected a wire bond arc of interest (the primary target wire bond #1 in Figure 3), the sample was then cross-sectioned using the propriety Perfect Edge process which combines a mechanical cutting step and inert gas plasma polishing. This process flow was developed to enable key micro-structural information to be extracted from samples with speed and a ccuracy, allowing us to target features within packages such as the SiP package studied here. Because the X-ray images provide excellent interior 3D information, there is no need for de-encapsulation prior to the physical cross-section.

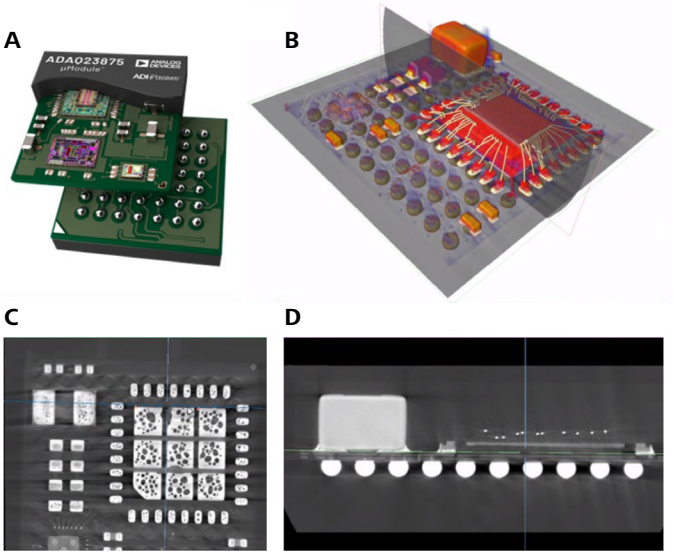

Figure 1 *3D X-ray tomography compared to schematic. A) Schematics of dissected SiP (marketing material) suggest the internal chips and electric net design. B) 3D color-rendering of acquired tomography shows internal wire bond networks in this study. C-D) examples of virtual cross-sections.*

The process allows us to minimize artifacts, optimize preparation process, and increase positioning accuracy, making it possible to reliably target features with the accuracy down to submicron. Figure 4 shows the cross-section SEM image of the target Au wire with the assistance of the XRM image (Figure 4 top). The entire gold wire loop is accurately sectioned and undamaged between ball and wedge bonds.

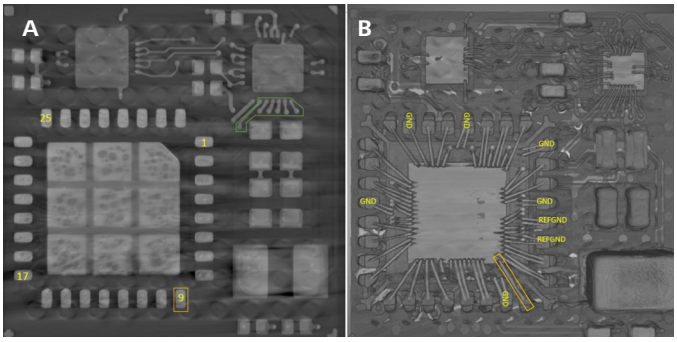

Figure 2 *The electric networks of interest with the suspicion of partial open (high resistance) are labeled on the planar views of 3D XRM images: A) bottom side view of the ADC (LTC2387-16). B) top side view.*

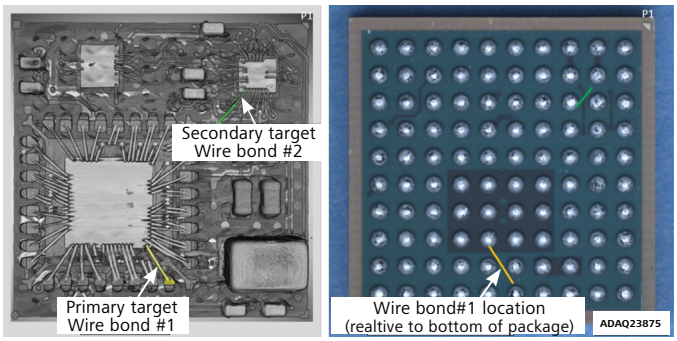

Figure 3 *Two target leads (labeled as yellow and green) were chosen in this study for demonstration purpose. The wire bonds lie at an oblique angle to the edge of the package. The photo on the right shows the positions of these two wires on an optical image.*

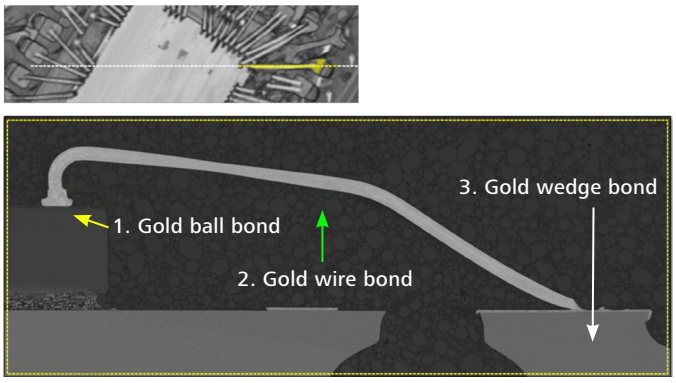

Figure 4 *An XRM virtual cross-section (top) and SEM image (below) show the entire targeted wire bond. The sample was analyzed to confirm the condition of electrical connectivity. The gold wire loop is undamaged between ball and wedge bonds.*

Because the Perfect Edge process provides a large surface free of contamination and distortion, we are able to acquire high-quality SEM images which reflect unaltered sample conditions. Figure 5 shows the ball bond made between gold wire and aluminum bond pad on the die. The moulded component body, wire bond and die are all clearly visible. Figure 6 shows that several phases of the intermetallic compounds (IMCs) were formed at the interface of the gold ball and the aluminum pad. IMCs provide physical and electrical connection between the wire and die. These IMC phases were further analzyed by Energy Dispersive Spectroscopy (EDS) in Figure 7. A thin layer of aluminum oxide (blue arrows in Figure 6-7) was formed between two IMC phases. A high-magnification image further confirms the oxide-rich region in Figure 8. We believe that this oxide layer could be the root cause of the excessive resistance observed during the overstress test, which is consistent to the report [6]. A further investigation is required to confirm that the oxide growth is responsible to the high resistance of the Au wire loop. As the main topic of this work is to develop the correlative sample preparation and imaging workflow, we continue to focus on the workflow.

HBM-Interposer Microbumps

A drawback of physical failure analysis is that the success rate strongly depends on how precisely the upstream non-destructive techniques can isolate and pinpoint the fault locations. Without accurate 3D geographic information, a failure region may be destroyed or altered during the PFA process, leading to no arrival of root causes. On a second case study, we choose an AMD Vega 64 2.5D interposer package as the test vehicle due to its multi-chip 3D stacks and large area (50 x 50 mm) silicon interposer connected with HBM using 20 µm Cu pillars and small volume solders. The complexity of the IC architecture challenges the conventional PFA workflows.

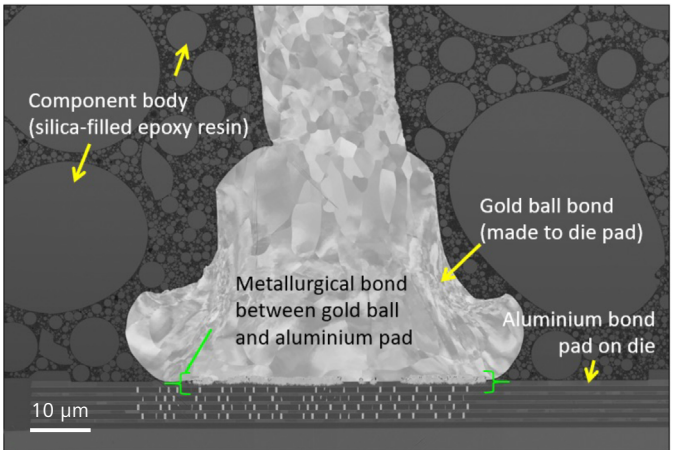

Figure 5 *Ball bond made between gold wire and aluminum bond pad. The moulded component, wire bond and die are all clearly visible. A metallurgical bond was formed between the gold and the aluminum during device manufacturing. This provides physical and electrical connection between the wire and die.*

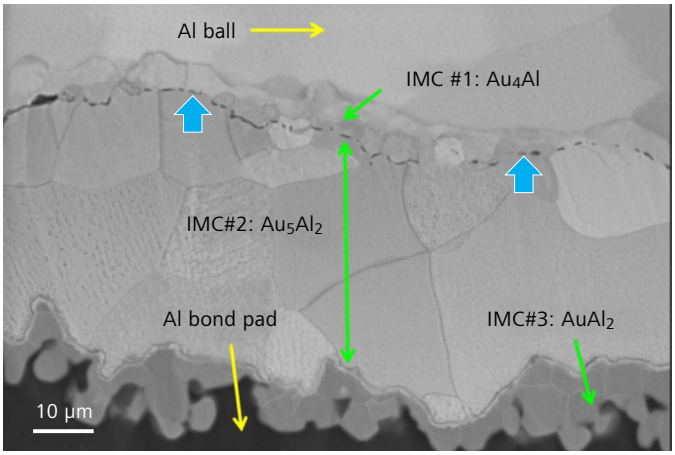

Figure 7 *Ball bond made between gold wire and aluminum bond pad. Several Au-Al IMC phases have formed. Energy Dispersive X-ray (EDS) analysis was used to identify the IMC phases (labelled here for reference).*

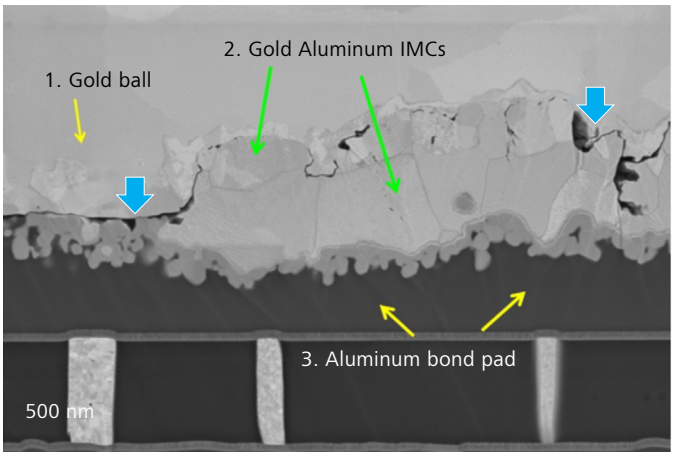

Figure 6 *Ball bond between gold wire and aluminum bond pad. Several Au-Al intermetallic compounds (IMC) phases have formed. IMCs can change over time in response to elevated temperature (solid-state diffusion). In severe cases, solid-state changes can cause de-bonding and bond failure.*

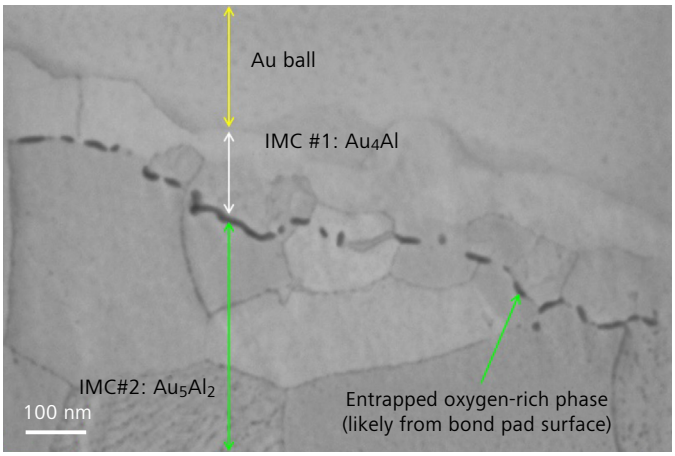

Figure 8 *Part of a ball bond made between gold wire and aluminum bond pad. Two Au-Al IMC phases have formed with a thin layer of oxygen-rich material between the two IMC phases.*

3D X-ray data was acquired with 90 kV energy at 0.7 µm/voxel resolution for the 2.5D package using XRM 4X optical objective. The fault region was microbump joint cracks at the interposer interface formed during thermal compression bonding process. The X-ray data clearly shows ~2 µm thick bump cracks in all three orientations (Figure 9b-d). With the information of the defect location in 3D to facilitate the sample preparation, physical cross-sectioning and SEM analysis followed to investigate possible root causes of the joint cracks. In this case, the Perfect Edge process was not employed. It is virtually impossible to do an accurate cross-section without the guidance of 3D X-ray data because the layer of the target microbumps are deeply buried, and therefore they are not visible by optical methods.

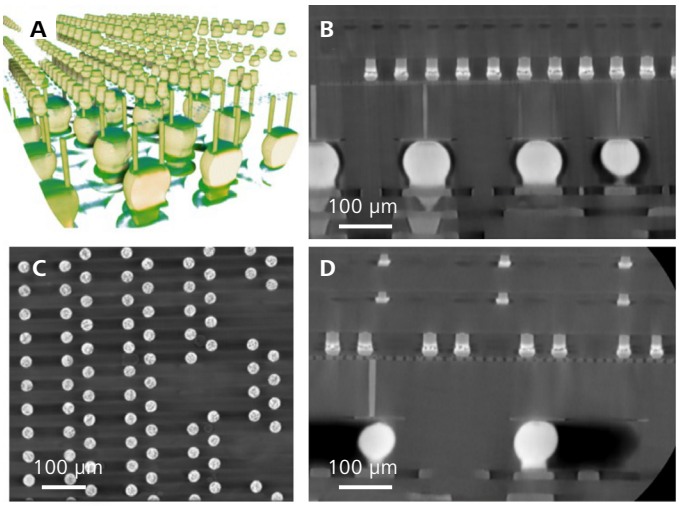

Figure 9 *3D X-ray tomographic images at 0.7µm/vox of the HBM 2.5D interposer package. A) 3D color-rendering image. B) Virtual slice shows the microbump layer between the Si interposer and HBM. C) planar view of the microbump layer. D) side view of the same layer of the microbumps.*

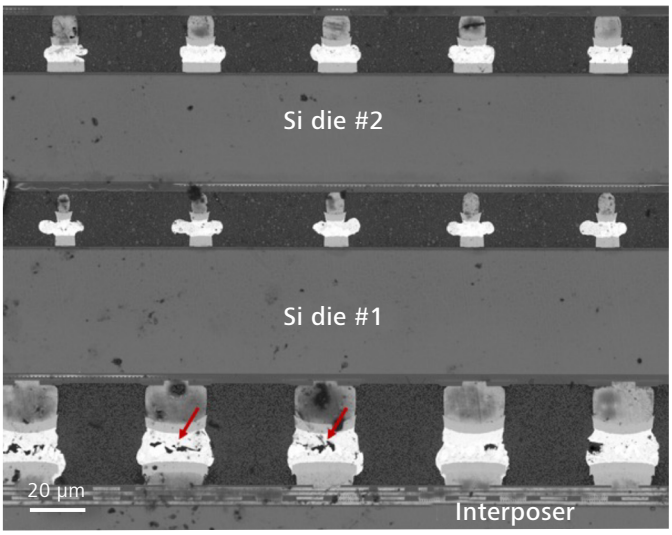

Figure 10 *Backscatter electron image of the microbump layer with two HBM die stacks on the top. The image was conducted with 5 kV acc. voltage at 86 nm/pixel.*

It is also not feasible to use the HBM bumps on the top layer as reference because they are not fully aligned with the target layer of microbumps in XY orientations (Figure 9d). To our best knowledge, XRM imaging is the only non-destructive technique which can reconstruct internal 3D structures of this package and provide sufficient resolution on the joint cracks.

Figure 10 shows a backscatter electron microscope image of the target bump layer at the bottom of the micrograph. Conducting imaging at 5 kV accelerating voltage in high vacuum using the pixel size of 86 nm, the microbump joint cracks (indicated by red arrows) are clearly visible during the sample cross-sectioning through the center of the target microbumps. This image validates the existence of µbump micro-cracks observed in 3D XRM images. Figure 11 shows an individual microbump with solder joint cracks. It seemed that Ni pad layers and Cu pillars were intact without any sign of failure. Several intermetallic compounds (IMCs) phases were observed on the target microbump (Figure 11b).

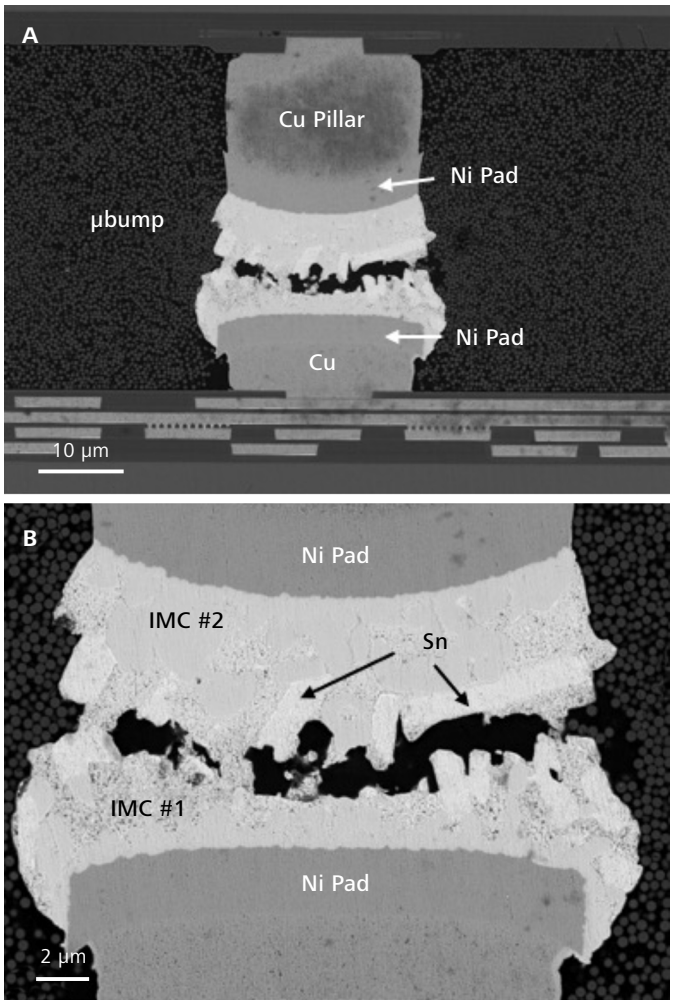

Figure 11 *Backscatter electron images of a microbump crack imaged at 5 kV acc. voltage with an annular backscatter detector. A) 37 nm/pixel; B) 15 nm/pixel.*

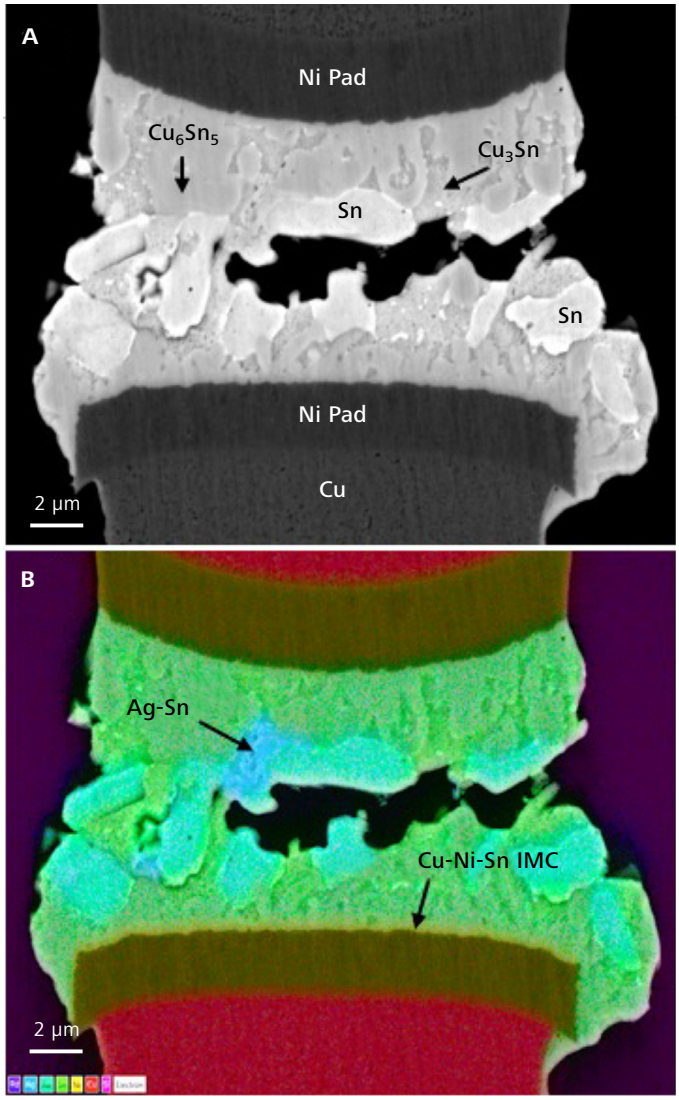

Figure 12 *Backscatter electron image and energy dispersive X-ray spectroscopy (EDS) elemental map of a cracked microbump with distinct metal phases in the solder and solder mask. The pixel size is 31 nm.*

The backscatter image in Figure 12a and the EDS elemental map image in Figure 12b show the cracked microbump with several metal phases in the solder materials. Analytical imaging conditions were 17 kV accelerating voltage with 3 nA beam current at a working distance of 8.5 mm, map live time 576 seconds using an EDS detector. We were able to identify the different IMC phases formed during thermal compression bonding assembly. Based on the X-ray data, SEM images, and EDS information on the bump metallurgy, we concluded that the large interposer warpage is likely to generate sufficient shear force on the microbump layer, leading to the crack formation and propagation. There was no other metallic abnormality observed in this case.

Conclusion

We demonstrated a correlative microscopic workflow that integrates XRM's non-destructive 3D imaging capability to PFA workflows, enabling analyzer to precisely locate and prepare defects of interest for nanoscale imaging and characterization with SEM. We investigated a wire bonding in a commercial SiP device and a microbump in a 2.5D interposer package to exemplify the microscopic workflow and the Perfect Edge process to prepare a pristine SEM surface. With more incoming challenges in effective defect isolation and localization for 3D packaging and heterogeneous integration, this workflow can be used to significantly improve the effectiveness of PFA workflows by providing highly accurate 3D information to guide the subsequent crosssections.

References

[1] L. Mirkarimi, A. Gu, L. Hunter, G. Guevara, M. Huynh, R. Katkar, "X-ray Microscopy and Root Cause Analysis in Electronic Packaging", *Proc 41st Int'l Symp for Testing and Failure Analysis,* Portland, OR, Nov. 2015, pp. 430-435. doi: 10.31399/asm.cp.istfa2015p0430

[2] A. Gu, A. Andreyev, M. Terada, B. Zee, S. M. Zulkifli, Y. Yang, "Accelerate Your 3D X-ray Failure Analysis by Deep Learning High Resolution Reconstruction Paper," Int'l Symp for Testing and Failure Analysis, No: istfa2021p0291, pp. 291-295, Phoenix, AZ, Dec 2021.

[3] S. M. Zulkifli, B. Zee, W. Qiu, A. Gu, "High-Res 3D X-ray Microscopy for Non-Destructive Failure Analysis of Chip-to-Chip Micro-bump Interconnects in Stacked Die Packages", *IEEE 24th Int'l Symp on the Physical and Failure Analysis of Integrated Circuits (IPFA),* Chengdu, China, Jul. 2017. doi:10.1109/IPFA.2017.8060111

[4] A. Gu, J. Auyoong, "3D Measurement Workflow for Packaging Development and Production Control Using High-Resolution 3D X-ray Microscope", *2018 IEEE 20th Electronics Packaging Tech Confer (EPTC),* Singapore, Dec. 2018. doi:10.1109/EPTC.2018.8654390

[5] Viswanathan and L. Jiao, "Developments in Advanced Packaging Failure Analysis using Correlated X-Ray Microscopy and LaserFIB," 2021 IEEE 23rd Electronics Packaging Technology Conference (EPTC), 2021, pp. 80-84, doi: 10.1109/EPTC53413.2021.9663938

[6] A. Gu, M. Terada, H. Stegmann, T. Rodgers, C. Fu and Y. Yang, "From System to Package to Interconnect: An Artificial Intelligence Powered 3D X-ray Imaging Solution for Semiconductor Package Structural Analysis and Correlative Microscopic Failure Analysis," IPFA 2022, Singapore

[7] Application Note, Materials Consultancy Services Ltd., Midlothian Innovation Centre, Midlothian, UK, 2020; https://www.themcsgroup.co.uk

[8] M. J. McCracken, "Assessing Au-Al Wire Bond Reliability Using Integrated Stress Sensors", MS thesis, University of Waterloo, Waterloo, Ontario, Canada, 2010

microscopy@zeiss.com
www.zeiss.com/semiconductor-microscopy